JPn Neuroscience

The Journal of Physiology

J Physiol 593.17 (2015) pp 3865–3884

Novel fluorescence resonance energy transfer-based reporter reveals differential calcineurin activation in neonatal and adult cardiomyocytes

Hojjat Bazzazi, Lingjie Sang, Ivy E. Dick, Rosy Joshi-Mukherjee, Wanjun Yang and David T. Yue*

Departments of Biomedical Engineering and Neuroscience, Centre for Cell Dynamics, Johns Hopkins University School of Medicine, Baltimore, MD, USA

Key points

- Novel fluorescence resonance energy transfer-based genetically encoded reporters of calcineurin are constructed by fusing the two subunits of calcineurin with P2A-based linkers retaining the expected native conformation of calcineurin.
- Calcineurin reporters display robust responses to calcium transients in HEK293 cells. The sensor responses are correlated with NFATc1 translocation dynamics in HEK293 cells.
- The sensors are uniformly distributed in neonatal myocytes and respond efficiently to single electrically evoked calcium transients and show cumulative activation at frequencies of 0.5 and 1 Hz.
- In adult myocytes, the calcineurin sensors appear to be localized to the cardiac z-lines, and respond to cumulative calcium transients at frequencies of 0.5 and 1 Hz.

Abstract The phosphatase calcineurin is a central component of many calcium signalling pathways, relaying calcium signals from the plasma membrane to the nucleus. It has critical functions in a multitude of systems, including immune, cardiac and neuronal. Given the widespread importance of calcineurin in both normal and pathological conditions, new tools that elucidate the spatiotemporal dynamics of calcineurin activity would be invaluable. Here we develop two separate genetically encoded fluorescence resonance energy transfer (FRET)-based sensors of calcineurin activation, DuoCaN and UniCaN. Both sensors showcase a large dynamic range and rapid response kinetics, differing primarily in the linker structure between the FRET pairs. Both sensors were calibrated in HEK293 cells and their responses correlated well with NFAT translocation to the nucleus, validating the biological relevance of the sensor readout. The sensors were subsequently expressed in neonatal rat ventricular myocytes and acutely isolated adult guinea pig ventricular myocytes. Both sensors demonstrated robust responses in myocytes and revealed kinetic differences in calcineurin activation during changes in pacing rate for neonatal versus adult myocytes. Finally, mathematical modelling combined with quantitative FRET measurements provided novel insights into the kinetics and integration of calcineurin activation in response to myocyte Ca transients. In all, DuoCaN and UniCaN stand as valuable new tools for understanding the role of calcineurin in normal and pathological signalling.

*Dr David Yue passed away on 23 December 2014. He was a deeply innovative and passionate scientist who will be greatly missed by all.

DOI: 10.1113/JP270510

(Received 1 April 2015; accepted after revision 16 June 2015; first published online 19 June 2015)
Corresponding author H. Bazzazi: Department of Biomedical Engineering, The Johns Hopkins University School of Medicine, Ross Building, Room 713, 720 Rutland Avenue, Baltimore, MD 21205, USA. Email: hbazzazi@jhmi.edu

Abbreviations aGPVM, adult guinea pig ventricular myocyte; CaM, calmodulin; CaNA, calcineurin-A; CaNB, calcineurin-B; DuoCaN, dual calcineurin sensor; FRET, fluorescence resonance energy transfer; NFAT, nuclear factor of activating T cells; NRVM, neonatal rate ventricular myocyte; UniCaN, unimolecular calcineurin sensor.

Introduction

The phosphatase calcineurin (PP2B) is a central component of many Ca^{2+}signalling pathways relaying elevated Ca^{2+} signals from the plasma membrane to the nucleus. Structurally, calcineurin comprises two subunits, a catalytic subunit calcineurin-A (CaNA, ∼60 kDa) and a calcium binding subunit calcineurin-B (CaNB, ∼19 kDa) which is structurally similar to calmodulin (CaM). CaNA contains a catalytic phosphatase domain, a Ca^{2+}/CaM binding domain, and an autoinhibitory domain that under basal calcium levels binds to and blocks the catalytic domain, preventing phosphatase activity (Li *et al.* 2011). The CaM-like CaNB subunit has four EF-hand domains capable of binding four calcium ions. The two calcium binding sites on the amino terminus bind calcium with high affinity and are occupied under basal calcium conditions (50–100 nM); by contrast, the two sites on the carboxy terminus bind calcium with lower affinity (K_d∼0.5 μM), and become occupied when intracellular calcium concentration ($[Ca^{2+}]_i$) rises, which together with Ca^{2+}/CaM binding activates calcineurin (Klee *et al.* 1979,1998; Aramburu *et al.* 2000; Rusnak & Mertz, 2000; Yang & Klee, 2000). Once active, calcineurin initiates downstream signalling pathwaysrequired for cell adaptation, function and survival (Rusnak & Mertz, 2000). One of the most well-studied of these pathways is the activation of nuclear factor of activating T cells (NFAT), a critical component of T cell activation and proper immune function (Durand *et al.* 1988; Shaw *et al.* 1988).

Although the immune system has been the classic context for discoveries regarding the calcineurin–NFAT pathway, this pathway is also critical for diverse biological functions including axonal growth (Graef *et al.* 2003), learning and memory (Graef *et al.* 1999), and synaptic cycling and plasticity in the CNS(Sun *et al.* 2010; Sanderson *et al.* 2012). Moreover, proper calcineurin signalling is essential for the development of a wide range of cell types and tissues, including normal cardiac development (de la Pompa *et al.* 1998; Ranger *et al.* 1998), cardiac myocyte differentiation (Kasahara *et al.* 2013), pancreatic beta cell growth and function (Heit *et al.* 2006), and Schwann cell differentiation (Kao *et al.* 2009). It has also been discovered that disruption of the CaNB1subunit in the heart results in abnormal cardiac growth, impaired systolic and diastolic functions, and mortality (Schaeffer *et al.* 2009; Wolska, 2009). Moreover, calcineurin inhibition is suggested for potential therapeutic intervention in heart failure (Sussman *et al.* 1998). The broad importance of calcineurin signalling in normal and pathological conditions underlines the value of new tools capable of measuring calcineurin activation with spatiotemporal precision in live primary cells. Here, we deploy just such a tool in cardiac myocytes, providing new insights into calcineurin dynamics in these cells. Traditional biochemical methods have been instrumental in elucidating the basic biology and structure of calcineurin activation in different cell types (Klee & Krinks, 1978; Klee *et al.* 1979,1998; Crabtree, 1989; Liu *et al.* 1991; Jain *et al.* 1993; Stemmer & Klee, 1994). However, these assays are generally destructive and provide limited spatiotemporal resolution. Recent developments in fluorescent-based genetically encoded sensors have opened new vistas into studying the complex dynamics of signalling pathways in live cells (Takao *et al.* 2005; Newman & Zhang, 2008; Mehta *et al.* 2014). These sensors utilize fluorescence resonance energy transfer (FRET) to quantify conformational changes of proteins associated with activation (Jares-Erijman & Jovin, 2003). Following this idea, we developed two genetically encoded FRET-based calcineurin activity reporters, based on native calcineurin subunits, which feature rapid kinetic responses and suitable dynamic ranges in response to calcium signals in cardiomyocytes.

Methods

Molecular biology

To ensure a 1:1 stoichiometry of our calcineurin subunits we utilized a viral-based 2A sequence derived from porcine tescho virus (P2A) (Robertson *et al.* 1985; Ryan *et al.* 1991). This creates a P2A site for autonomous separation of the expressed fusion protein during translation, mimicking the normal expression of CaNA and CaNB as separate proteins. First, plasmids were created with several P2A sequence variations linking Cerulean and Venus. Cerulean was cloned into pCDNA3 (Clontech) using the *Kpn*I and *Bam*HI sites. Venus was then PCR amplified using a primer containing the P2A sequence and the product was cloned into the *Not*I and *Xba*I sites of the Cerulean pCDNA3 plasmid. This intermediate Cer-P2A-Ven plasmid was used to test cellular P2A hydrolysis, and the final sequence FQGPGATNFSLLKQAGDVEENPGPSLSK was chosen for

creating the DuoCaN sensor. The underlined portion delineates P2A itself, with a flanking N-terminal sequence as indicated.

The Cer-P2A-Ven plasmid was then used to make the final DuoCaN plasmid using the plasmid pET15b CaNA-CaNB, a generous gift from Dr Anjana Rao (Addgene plasmid no. 11787). Calcineurin B was PCR amplified and cloned into the *Bam*HI and *Not*I sites, and calcineurin A was PCR amplified and inserted into the *Xho*I and *Xba*I sites, replacing the existing Venus. Finally, Venus was cloned into the *Xba*I and *Apa*I sites, with a stop codon (TAA) preceding the *Apa*I site. This sensor should be cleaved between CaNA and CaNB after translation. The UniCaN sensor was constructed by the same method except that a modified mutated form of the P2A sequence was contained in the primer. The mutation consisted of a quadruple alanine substitution on the consensus P2A sequence (NPGP to AAAA). For adeno viral expression, sensors were sub-cloned into a pAdLox vector (Hardy *et al.* 1997) as follows: Venus was PCR amplified and ligated into the pAdLox via *Xba*I and *Eco*RI. PCR was then used to amplify the Cerulean-containing portion of DuoCaN or UniCaN (CER-CnB-P2Asequence-CnA) and the segment was ligated into the Venus-pAdLox plasmid using *Sal*I and *Xba*I.

The mCherry-NFATc1 construct was made by inserting mCherry (Shaner *et al.* 2004) into human NFATc1 (Beals *et al.* 1997) which was a generous gift from Dr Gerald R. Crabtree (Addgene plasmid no. 24219) using *Hind*III and *Bam*HI. The resulting mCherry-NFATc1 fusion construct was then subcloned into pcDNA3 via *Xho*I and *Xba*I.

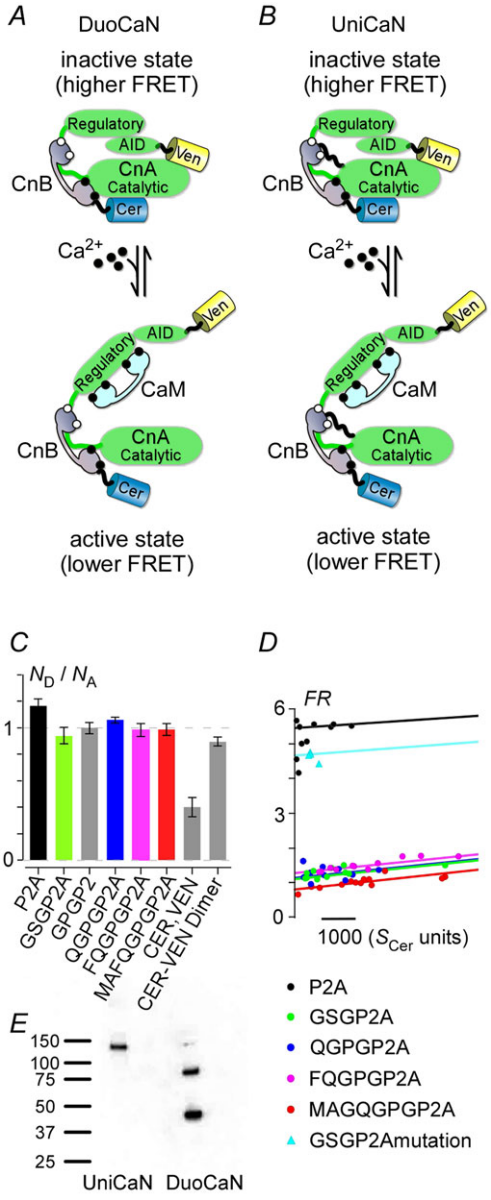

Figure 1. The design of DuoCaN and UniCaN sensors of calcineurin activation
A, dual calcineurin sensor (DuoCaN) was constructed by joining a Cerulean (Cer)-tagged CaNB1 and a Venus (Ven)-tagged CaNAα, using a P2A-based linker. The P2A-based linker undergoes a self-hydrolysis reaction at the translational level, resulting in complete dissociation of the linked partners at the 2A site. *B*, unimolecular calcineurin sensor (UniCaN) was constructed in the same way as DuoCaN, except the P2A-based linker was mutated so that no self-hydrolysis occurred. Cand*D*, analysis of the cleavage efficiency of the P2A peptides by 3^3-FRET.C, the ratio of donor (Cer) to acceptor (Ven) molecules was computed. Several P2A linkers, with variable N-terminal flanking sequences, were tested. C-V dimer was used as a control for no cleavage and 1:1 stoichiometry, and C,V (denoting the co-transfection of individual Cerulean and Venus) was used as a control for complete separation and altered stoichiometry (grey). All tested P2A constructs showed 1:1 stoichiometry. Error bars indicate SEM (n = 5–8) for all constructs. *D*, FRET ratio (*FR*) was plotted against Cerulean fluorescence. Low *FR* values (around 1) indicate complete fluorophore separation, as seen for all the P2A linkers with flanking N-terminal sequence additions. High *FR* values (>5) indicate no fluorophore separation, as is the case for the P2A sequence with no sequence additions (Cer-P2A-Ven, black) and the quadruple P2A mutant (NPGP to AAAA, cyan triangles). *E*, Western blot of HEK293 cell lysates probed with anti-GFP antibody. UniCaN, a single band at ~130 kDa; DuoCaN, two bands at 45 and 85 kDa.

Transfection into HEK293 cells

For calcium calibration of sensors and NFAT translocation experiments, HEK293 cells were cultured in glass-bottom dishes (In Vitro Scientific, Sunnyvale, CA, USA). The sensor constructs were transiently transfected using the Fugene transfection reagent (Promega, Madison, WI, USA) and the cells were imaged 24 h after transfection. For calcium calibration experiments, we applied 0.5–1 μg of the sensor construct. For translocation experiments, 1 μg of mCherry-NFAT and 1 μg of either UniCaN or DuoCaN were co-transfected ~36 h before the experiment.

Virus production

Adenoviral vectors were generated using the Cre-Lox recombination system as previously described (Alseikhan *et al.* 2002; Colecraft *et al.* 2002; Limpitikul *et al.* 2014). Briefly, the DuoCaN and UniCaN pAdLox plasmids were co-transfected along with the $\psi 5$ vector into Cre8 cells allowing for expression and packaging of the viral particles. After three rounds of expansion in Cre8 cells, the viral particles were amplified in HEK293 cells and purified via a standard CsCl gradient protocol generating virus with a titre greater than 10^{10} particles/μl.

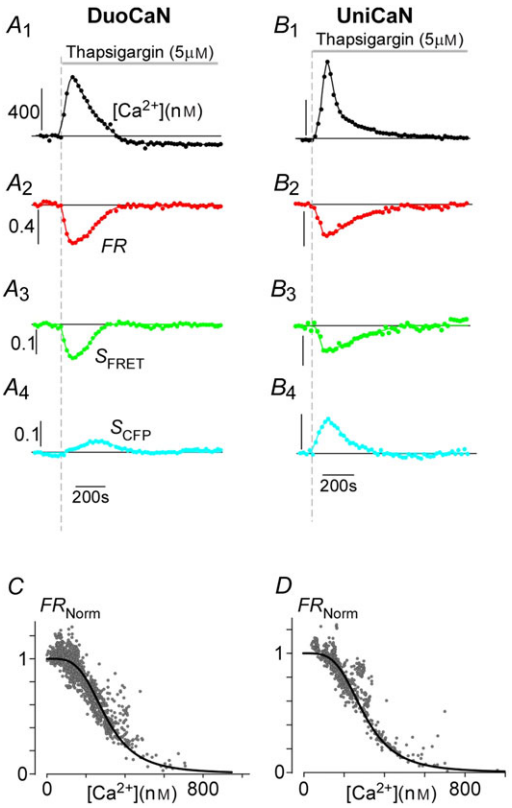

Figure 2. The FRET changes in DuoCaN and UniCaN sensors in response to thapsigargin-induced calcium transients
A, exemplar DuoCaN response to 1 μM thapsigargin in the presence of 200 μM extracellular $[Ca^{2+}]$. A_1, thapsigargin elicits a large calcium transient as recorded with the indo-1 calcium dye. Scale bar indicates calcium concentration in nM. A_2, there is a ~40% change in the FRET ratio (*FR*) for DuoCaN. Scale bar indicates the normalized response of the sensor. The FRET channel signal decreases (A_3), while the CFP channel signal increases consistent with the expected conformational changes in calcineurin complex. *B*, exemplar UniCaN response to thapsigargin with 200 μM extracellular $[Ca^{2+}]$.B_1, calcium transient as recorded by indo-1.B_2, the corresponding change in $\bar{R}_{sensor}$ is ~40%. B_3, FRET signal has a downward transient, while, B_4, the CFP signal shows an upward transient.Cand*D*, quasi steady-state calcium calibration of DuoCaN (*C*, data from 18 cells) and UniCaN (*D*, data from 13 cells). Both population data points were fitted by a Hill equation with a Hill coefficient of $n = 3.8$ and $K_D = 300$ nM (the continuous line is described by $FR_{Norm} = \frac{1}{1+([Ca]/300)^{3.8}}$).

Myocyte culture

Neonatal rat ventricular myocytes (NRVMs) were isolated using standard protocols (Chlopcikova *et al.* 2001; Tung & Zhang, 2006) and plated on glass coverslips for 3–7 days prior to imaging. Adenoviruses containing either DuoCaN or UniCaN were added 24 h prior to imaging the myocytes. Adult guinea pig ventricular myocytes (aGPVMs) were isolated as described (Joshi-Mukherjee *et al.* 2013) and plated on laminin-coated glass coverslips in M199 media containing 20% fetal bovine serum (FBS). After 1 h, media were exchanged with 0% FBS M199 media and DuoCaN or UniCaN viruses were added. Eight to 12 h later, the myocytes were washed once with warmed PBS, and the media were replaced with fresh 0% FBS media. aGPVMs were imaged within 32 h of plating.

FRET/Ca co-imaging and Ca^{2+} calibration experiments

HEK293 cells expressing DuoCaN or UniCaN were loaded with 1 μM indo-1AM (Sigma-Aldrich, St Louis, MO, USA) as previously described (Tay *et al.* 2007). For Ca^{2+} calibration experiments, the cells were placed in Tyrode's solution of varying external $[Ca^{2+}]$ (0, 100, 200 and 300 μM) to vary the amplitude of the $[Ca^{2+}]_i$ rise induced by activating store-operated calcium entry portals. Calcium-free Tyrode buffered with 1 mM EGTA was used to elicit low-amplitude calcium transients. By plotting the cells with variable Ca^{2+} transient amplitudes we were able to populate the FRET/calcium calibration curves for UniCaN and DuoCaN. In HEK 293 cells, the transformation from indo-1 ratio to $[Ca^{2+}]$ (Grynkiewicz *et al.* 1985) is given by the following relation:

$$\bar{R}_{indo} = \frac{F_{405}}{F_{485}} \qquad \left[Ca^{2+}\right](\mathrm{nM}) = \beta K_D \frac{\bar{R}_{indo} - \bar{R}_{indo,min}}{\bar{R}_{indo,max} - \bar{R}_{indo}}$$

where $\beta = 2.14$, $K_D = 800$nM, $\bar{R}_{indo,min} = 0.44$, $\bar{R}_{indo,max} = 2.92$.

For calcineurin activation–calcium calibrations, the FRET ratio (*FR*)was normalized as follows:

$$FR_{Norm} = \frac{FR - FR_{min}}{FR_{max} - FR_{min}}$$

Recordings were done in a Tyrode's solution consisting of 138 mM NaCl, 4 mM KCl, 1 mM $MgCl_2$, 10 mM Hepes (pH 7.35 with NaOH) and 5 mM gluocose (all from Sigma-Aldrich). For direct $[Ca^{2+}]_i$ measurements in NRVMs, the myocytes were incubated for 30 min with 1 μM indo-1AM along with 20% pluronic acid at 37°C.

aGPVMs were loaded more readily and required only a 5 min incubation with 1 μM indo-1AM + 20% pluronic acid at room temperature. Electrical field stimulation was performed using a grass stimulator with platinum electrodes positioned ∼1 mm apart. The voltage amplitude for efficient field stimulation was in the range 10–20 V with a duration of 20–50 ms. Mechanical contraction of the cells under microscopic observation was used as an indicator for successful field stimulation. Calcium transients were recorded in response to electrical stimulation using 340 nm excitation and emission at both 405 and 485 nm. The UV excitation wavelength of indo-1 ensured no cross-talk with Cer fluorescence or FRET measurements. The normalized 405/485 nm fluorescence ratio ($\bar{R}_{indo}$) was used to infer $[Ca^{2+}]_i$. For DuoCaN and UniCaN recordings, cells were excited at 440 nm, and FRET emission was recorded at 530 nm, while CFP emission was recorded at 480 nm. The normalized FRET/CFP intensity ratio, $\bar{R}_{sensor} = \bar{S}_{FRET}/\bar{S}_{CFP}$ was used as a measure of calcineurin activity, where $\bar{S}_{FRET}$ and $\bar{S}_{CFP}$ are the normalized intensities for FRET and CFP signals, respectively.

Indo-1 traces were low-pass filtered with a 20 kHz cutoff frequency, while the same filtering algorithm was performed on individual CFP and FRET traces with a 5 kHz cutoff. This filtering did not alter the FRET response of the sensors. The transient reduction in FRET and the corresponding rise in CFP signals in response to electrical stimulation were clearly identifiable from the raw traces. Bleaching in individual CFP and FRET channel signals (attributable to bleaching of CFP due to prolonged excitation) was corrected for by fitting an exponential function to the signal baseline. This bleaching effect, however, was mostly absent after taking the ratio of the signals to obtain $\bar{R}_{sensor}$ and did not alter the final sensor response. The stimulation protocol included initial and final silent periods (no stimulation) which clearly indicated the baseline and bleaching effects, making fitting of the baselines straightforward. All analysis and data acquisition were performed with custom written software in MATLAB (Mathworks, Natick, MA, USA).

NFAT imaging

For NFAT translocation experiments, calcium-free Tyrode solution was used to achieve a low level of NFAT translocation and populate the lower part of the translocation-sensor response curve. Tyrode solution containing variable $[Ca^{2+}]$ (100, 200 or 300 μM) was used to achieve intermediate and complete NFAT translocation in order to populate the upper part of the correlation curve. Co-imaging of either DuoCaN or UniCaN with mCherry-NFATc1 was performed at 37°C with an LSM780 (Carl Zeiss, Oberkochen, Germany) confocal microscope with a mounted temperature-controlled chamber. All subsequent analysis and quantification of the sensor and NFATc1 translocation images were performed using ImageJ software (Schneider *et al.* 2012). NFAT translocation was quantified by the fraction of mCherry intensity in the nucleus versus the total whole-cell intensity using two-dimensional confocal images ($mCherry_{Nuclear}/mCherry_{Total}$). For time-lapse images, the imaging data were gathered every 30 s. Thapsigargin at 1 μM was added to the solution after 10–15 min of baseline imaging. This initial delay was included to obtain a sufficient fluorescence baseline.

Mathematical model of calcineurin activation

To capture the essential biology of calcineurin activation without increasing the number of parameters, we opted for a reduced version of a previously published model (Saucerman & Bers, 2008) that fitted our experimental data well. The following kinetic scheme describes the binding of four Ca^{2+} ions to CaM and of two Ca^{2+} to CaNB, and the subsequent binding of Ca^{2+}/CaM to the calcineurin complex:

$$2Ca + CaM \leftrightarrow Ca_2CaM$$
$$2Ca + Ca_2CaM \leftrightarrow Ca_4CaM$$
$$2Ca + Ca_2CN \leftrightarrow Ca_4CN$$
$$Ca_4CaM + Ca_4CN \leftrightarrow Ca_4CaMCa_4CN$$

The two conserved parameters are the free available CaM and free calcineurin:

$$C_1 = [CaM] + [Ca_2CaM] + [Ca_4CaM] + [Ca_4CaMCa_4CN] = [CaM]_0$$

$$C_2 = [Ca_2CN] + [Ca_4CN] + [Ca_4CaMCa_4CN] = [Ca_2CN]_0$$

Implying that C_1 and C_2 denote the available free CaM and calcineurin in the system.

The system of one-dimensional equations corresponding to the above reactions was solved in MATLAB (Mathworks). The following relation was used to fit the DuoCaN sensor data:

$$1 - \frac{\bar{R}_{sensor}}{R_0} = \alpha[Ca_4CN] + \beta[Ca_4CaMCa_4CN]$$

The values of the model parameters are tabulated in Table 1.

Quantification of the relative ratio of donor and acceptor molecules

FRET measurements for determining the stoichiometry of Cer to Ven-tagged molecules utilized the 3^3-FRET method

Table 1. Parameters of the mathematical model of calcineurin activation

Parameter	Description (value)	Reference
k_{20}	Off kinetics of 2 Ca^{2+} binding to apoCaM (10 s^{-1})	Saucerman & Bers (2008)
k_{02}	On kinetics of 2 Ca^{2+} binding to apoCaM (10 μM^{-2} s^{-1})	
K_{d02}	1 μM^2	Fit
k_{42}	Off kinetics of 2 Ca^{2+} binding to Ca^2CaM (1000 s^{-1})	Saucerman & Bers (2008)
k_{24}	On kinetics of 2 Ca^{2+} binding to Ca^2CaM (100 μM^{-2} s^{-1})	
K_{d42}	10 μM^2	Fit
$K_{D,CnA}$	The dissociation constant for the binding of Ca^{2+}/CaM to CN (100 pM)	Fit
$k_{off,CnA}$	Off kinetics of Ca^{2+}/CaM binding to CN (1 s^{-1})	Fit
$k_{on,CnA}$	On kinetics of Ca^{2+}/CaM binding to CN (10^4 μM^{-1} s^{-1})	
$K_{off,CnB}$	The on kinetics of 2 Ca^{2+} binding to CaNB (1 s^{-1})	Fit
$K_{D,CnB}$	0.5 μM^2	Saucerman & Bers (2008)
$k_{on,CnB}$	2 μM^{-2} s^{-1}	
C_1	Free available CaM	Fit
C_2	Free available CN	Fit
α	0.1	Fit
β	1	Fit

(Erickson *et al.* 2001,2003), which we briefly describe here. The band-pass filters for the FRET cube were centred at 440nm (excitation) and 535 nm (emission). Signals measured with this cube have three components: donor fluorescence due to direct excitation, acceptor fluorescence due to direct excitation and acceptor fluorescence due to FRET. To determine the relative intensity of donor and acceptor fluorescence due to direct excitation, fluorescence signals due to indirect excitation need to be determined and removed. To accomplish this, constants R_{D1} (CFP crosstalk in the FRET cube), andR_{A1} (YFP crosstalk in the CFP signal) must be obtained. These are readily obtained as follows: for R_{D1}, CFP is excited at 440 nm and emission at 535 nm is normalized by the emission at 480 nm. For R_{A1}, the emission of YFP at 480 nm due to 440 nm excitation is normalized by the emission in response to a 515 nm excitation. This scheme allows the isolation of the pure FRET signals according the following:

$$\text{Cerulean}_{\text{FRET}}\ (440,\ 535,\ \text{direct}) = R_{D1} \cdot S_{CFP}\ (\text{DA},\ 440,\ 480)$$

$$\text{Venus}_{\text{FRET}}\ (440,\ 535,\ \text{direct}) = R_{A1} \cdot [S_{YFP}\ (\text{DA},\ 500,\ 530\text{LP})]$$

To utilize these pure FRET signals to obtain the number of donor and acceptor molecules we utilize the following equations:

$$\text{Venus}_{\text{FRET}}\ (440,\ 535,\ \text{direct}) \approx N_A \cdot I_o \cdot G_{\text{FRET}}\ (\text{A},\ 440) \cdot F_{\text{FRET}}\ (\text{A},\ 535)$$

$$\text{Cerulean}_{\text{FRET}}\ (440,\ 535,\ \text{direct}) \approx N_D \cdot I_o \cdot G_{\text{FRET}}\ (\text{D},\ 440) \cdot F_{\text{FRET}}\ (\text{D},\ 535)$$

where G_{FRET} is the average molar extinction coefficient of the acceptor (Venus) over the wavelength range 430–450nm for a given optical setup and $F_{\text{FRET}}$is a parameter that incorporates the optical properties of the emission pathway. For more in-depths detail please see Erickson *et al.*(2001,2003).

Results

Design of FRET-based genetically encoded calcineurin reporters

To design robust calcineurin sensors, we exploited the conformational changes in calcineurin which occur following a rise in intracellular calcium. Full activation of calcineurin involves the displacement of the autoinhibitory domain by Ca^{2+}-CaM binding and Ca^{2+}-induced CaNB–CaNA changes, resulting in altered FRET (Fig. 1*A*). We hypothesized that these conformational changes would be detectable by FRET and proceeded to fuse Cerulean (Cer) to the amino terminus of CaNB (CaNB1 isoform) and Venus (Ven) to the carboxy terminus of CaNA (CaNAα isoform) (Mondragon *et al.* 1997) (Fig. 1*A*, *B*). To preserve the native 1:1 stoichiometry between CaNB1 and CaNAα, viral-based 2A sequences were employed as linker between the two calcineurin subunits (Robertson *et al.* 1985). These 2A sequences have been shown to undergo a self-hydrolysis reaction at the translational level, resulting in complete dissociation at the 2A site (Donnelly *et al.* 2001). The 2A sequence

derived from porcine tescho virus (P2A) (Robertson *et al.* 1985; Ryan *et al.* 1991) was utilized as the linker for the calcineurin sensor. To optimize the effectiveness of P2A, several C–V dimer constructs with different P2A linkers between the two fluorophores were made. The self-processing efficacy of these P2A linkers was tested in live cells by utilizing a 3^3-FRET assay and by computing the number of expressed donor (Cer) and acceptor molecules (Ven) as previously described (Erickson *et al.* 2001,2003) and briefly described in the Methods section. Figure 1*C* shows the ratio of donor to acceptor molecules (N_D and N_A, respectively) for various forms of the P2A linker. Reassuringly, the ratio is nearly 1 for all the P2A constructs, indicating 1:1 stoichiometry.

To investigate whether the P2A linkers between Cer and Ven were fully hydrolyzed under basal conditions, the FRET ratio (*FR*) was plotted against the Cer fluorescence intensity (Fig. 1*D*). All P2A linkers with a flanking amino terminal sequence had *FR* values close to 1 (as there is no inherent protein–protein interaction between Cer and Ven), indicating that the fluorescent proteins were completely separated. In contrast, the P2A sequence without the flanking amino terminal sequences (black) failed to cleave (high *FR*), consistent with previous observations (Szymczak *et al.* 2004; Kim *et al.* 2011). To confirm the efficiency of the P2A sequences, Fig. 1*E* shows the result of a Western blot of the sensors expressed in HEK293 cells using an anti-GFP antibody. The complete processing of DuoCaN is demonstrated by the two bands corresponding to Cer-CnB (lower band, ~46 kDa molecular weight) and CnA-Ven (upper band, ~87 kDa molecular weight). Reassuringly, UniCaN does not cleave and yields a single band (molecular weight of 133 kDa). Given the successful cleavage of all the P2A variants, we opted to use the FQGPGP2A sequence to avoid the introduction of an inner methionine in the sensor. In addition, a quadruple alanine substitution within the consensus carboxy terminal NPGP consensus sequence (NPGP to AAAA) abolished the function of P2A and resulted in high *FR* values (Fig. 1*D* cyan triangles).

Two sensors were constructed based on these findings. The first variant, called DuoCaN (dual calcineurin sensor, Fig. 1*A*), was based on the FQGPGP2A sequence, which is fully severed inside cells. The second type of sensor, called UniCaN (unimolecular calcineurin sensor, Fig. 1*B*), was constructed by using the quadruple alanine mutant form of the P2A sequence, which is non-functional (Fig. 1*D*). DuoCaN is expected to be closer to the native conformation in cells, making it a valuable tool for assaying calcineurin dynamics under physiological conditions. However, targeting DuoCaN to different subcellular locations would be challenging. UniCaN circumvents this problem by fusing the two subunits together. Thus, the two sensors are complementary in their use.

Calibrating the calcium response of the sensors

Indo-1 was utilized to simultaneously measure $[Ca^{2+}]_i$ and FRET responses of the sensors in HEK293 cells. Slow calcium transients were elicited by applying thapsigargin to activate store-operated Ca^{2+} influx. There was variability in calcium amplitudes elicited with thapsigargin even with the same extracellular Ca^{2+} (e.g. 200 μM). However, wider variations of calcium transient amplitudes were obtained by varying the external calcium concentration within the range 0–300 μM, thus fully populating the calibration curves. Figure 2*A* demonstrates the sensor response to thapsigargin-induced calcium transients for DuoCaN. The resultant calcium transient (Fig. 2A_1) activates calcineurin, which manifests as a

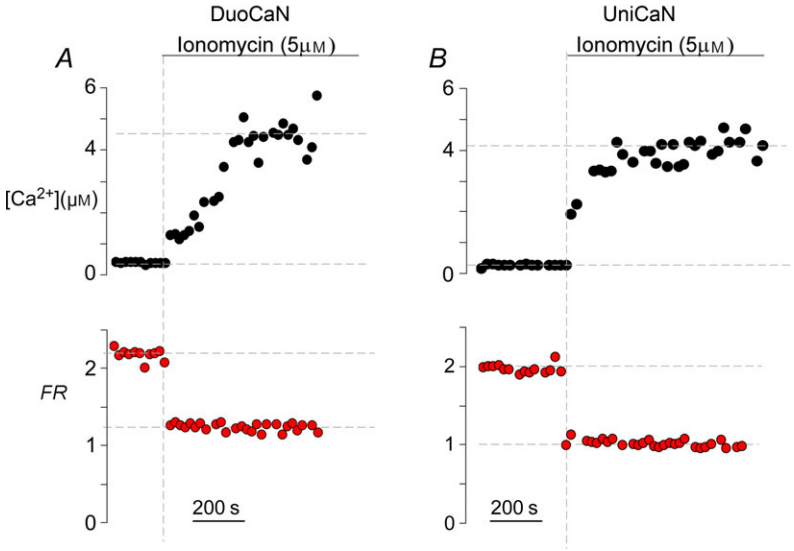

Figure 3. Sensor response in the presence of CaM overexpression
DuoCaN (*A*) and UniCaN (B*)* activation in response to 10 μM ionomycin in HEK293 cells overexpressing wild-type CaM. Simultaneous recording of the Ca^{2+} concentration (black) via indo1-AM and sensor response (red) demonstrating a large dynamic range of each calcineurin sensor in the presence of excess CaM and 2 mM extracellular $[Ca^{2+}]$.

decrease in the normalized *FR* of DuoCaN (Fig. 2A_2). The corresponding FRET signal (Fig. 2A_3) decreases while the CFP signal increases (Fig. 2A_4). The *FR* value then returns to basal level following the decay of the calcium transient. Figure 2*B* demonstrates a similar response for the UniCaN sensor, where the *FR* value, as well as FRET, and CFP signals follow the calcium transient. Both DuoCaN and UniCaN respond to the calcium transient with a ∼40% response. Remarkably, this response approaches 100%, when ionomycin is applied to HEK

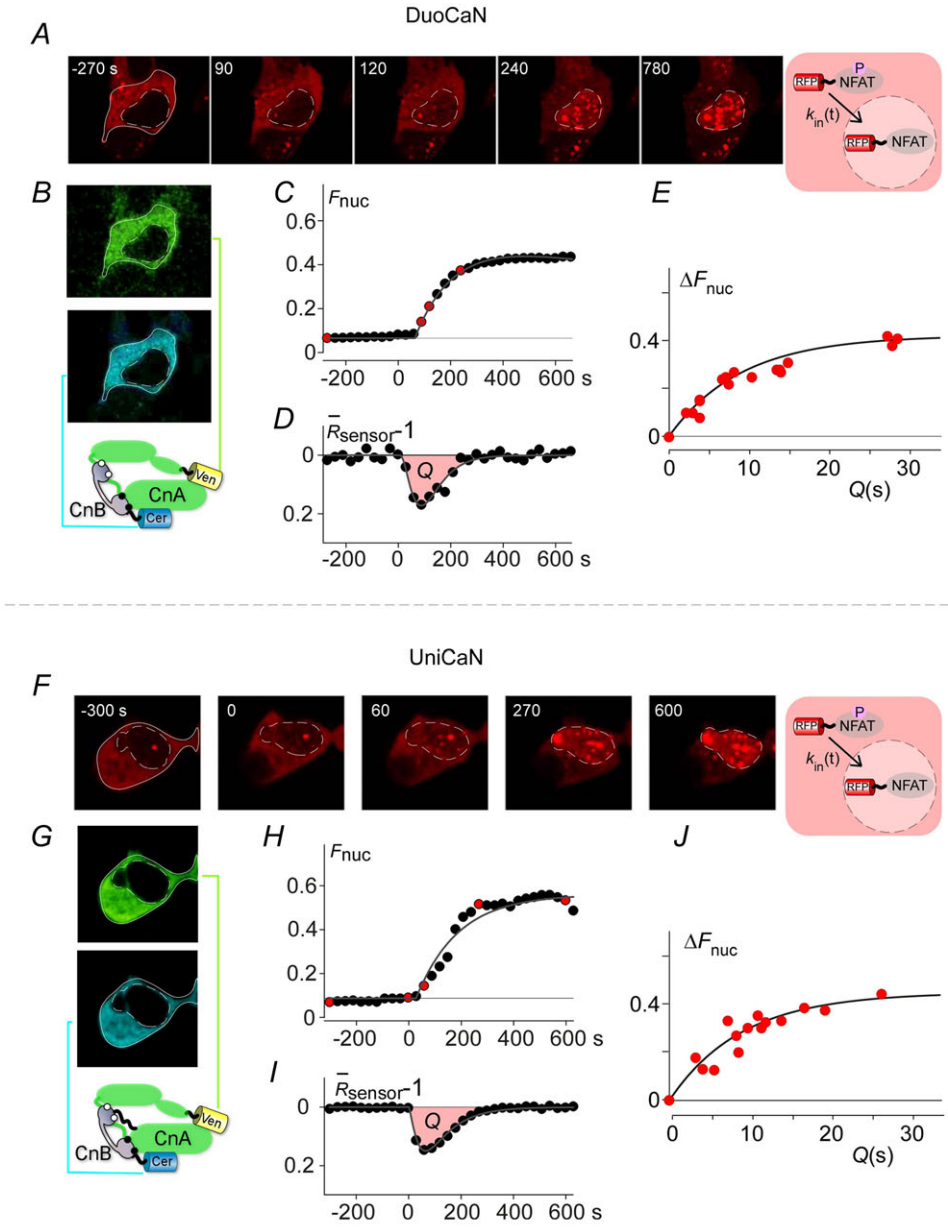

Figure 4. Correlation of sensor activation to calcineurin activity via NFATc1 nuclear translocation dynamics
A, time-lapse imaging of mCherry-NFAT nuclear translocation induced by thapsigargin for DuoCaN. The boundary of the cell is indicated the solid white line, and its nucleus outline was drawn by the dashed white line. CFP and FRET channel imaging of the DuoCaN sensor. *C*, thapsigargin induced NFAT translocation for an exemplar in 200 μM extracellular Ca^{2+} ($\Delta F_{nuc} = 0.45$). *D*, the simultaneous sensor activation profile of DuoCaN.*Q* denotes the area under the curve of the sensor activation profile. *E*, correlation between the total change in nuclear NFAT (ΔF_{nuc}) and *Q* for DuoCaN ($n = 16$). Each red circle represents data from a single cell. Data were fitted by the equation $\Delta F_{nuc} = A\,(1 - e^{-Q/9})$ with $A = 0.42$. *F–J*, UniCaN results in the same format as *A–E*. *J*, $n = 15$ and $A = 0.45$ for UniCaN.

cells in which CaM is overexpressed (Fig. 3), indicating a considerable dynamic range of the sensors. Because the thapsigargin-induced calcium transients develop and decay slowly, it is reasonable to assume that the calcium–calcineurin system stays near a quasi-equilibrium state. Assuming that HEK293 cells have enough free CaM to activate the sensor (a reasonable assumption based on a previous study utilizing a FRET-based CaM sensor in HEK293 cells; Liu *et al.* 2010), this feature of the system can be exploited to calibrate *FR* with $[Ca^{2+}]_i$. This is akin to phase-plane analysis of dynamical systems where the two time-varying states are plotted against each other (here FR_{Norm} and calcium concentration, $[Ca^{2+}]$ as determined from indo-1 measurements). Accordingly, we plotted normalized *FR* ($\frac{FR-FR_{min}}{FR_{max}-FR_{min}}$) versus $[Ca^{2+}]$ at multiple time points for each cell (Fig. 2*C* for DuoCaN and Fig. 2*D* for UniCaN). The population data for both types of sensors were well fitted by a Hill

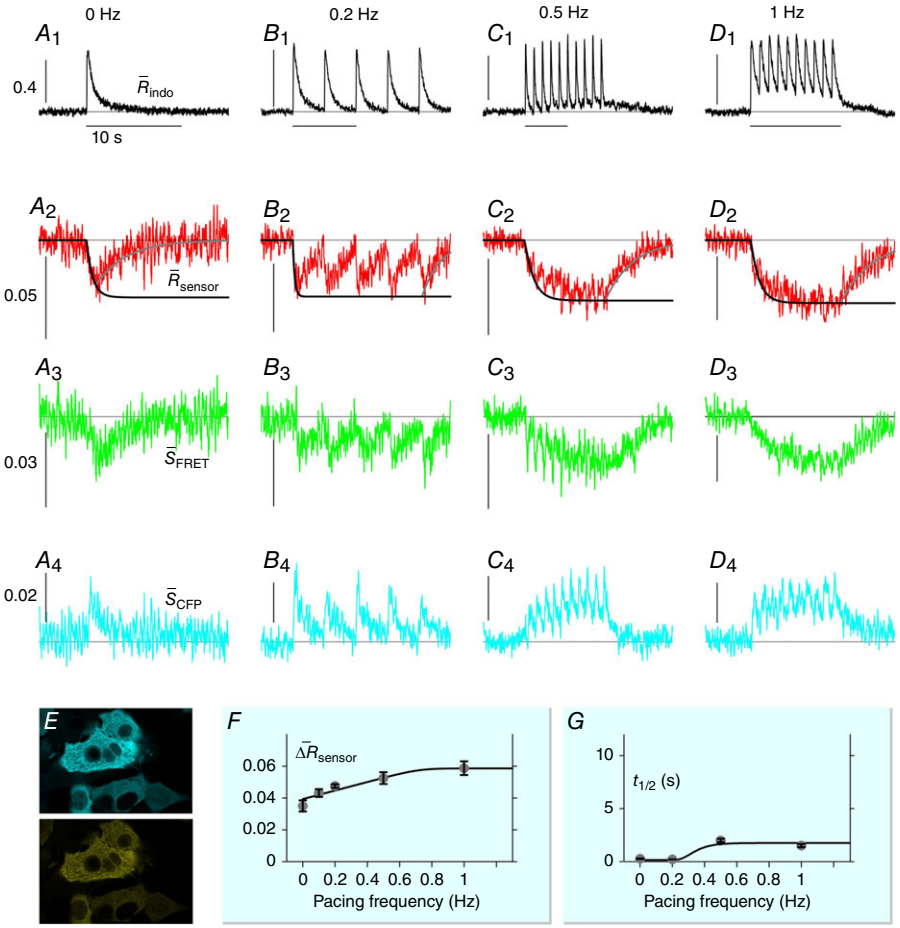

Figure 5. DuoCaN responding to electrical stimulations in NRVMs
A–D, indo-1 assayed calcium transients along with the normalized fluorescence signals for an exemplar cell. *A*, the indo-1 response elicited by a single stimulation pulse (A_1, black trace), the change in $\bar{R}_{sensor}$ is shown (A_2, red), along with a fit to the activation (solid black) and inactivation signal components (solid grey). The scale bar indicates the normalized response here and throughout. *B*, indo-1 signal is shown for the 0.2 Hz pacing (black, B_1)with concurrent decrease in $\bar{R}_{sensor}$(B_2). The individual channels respond consistently, the FRET channel (B_3, S_{FRET}, green) decreases while the CFP channel increases (B_4, S_{CFP}, cyan). *C*, following a 10 s silent period, the cell was paced at 0.5 Hz for 10 s with the calcium transients shown (C_1, black). *FR* response is shown (C_2, red). Motion artifacts are present in the FRET (C_3, green) and CFP signals (C_4, cyan), which are corrected by the ratio (C_2). *D*, the cell is paced at 1 Hz for 10 s following a silent period of 5 s (D_1, black), leading to cumulative activation of the sensor (D_2, red) simultaneous decrease in FRET signals (D_3, green) and increase in CFP signals (D_4, cyan). *E*, DuoCaN expression and cellular distribution in NRVMs, assessed by imaging through CFP channel (top, cyan) and FRET channel (bottom yellow). *F*, population average of normalized amplitude of sensor activation (solid grey circles, each circle representing n~5–10 cells, error bars indicate SEM) is plotted against simulation frequencies, showing a slow increase from ~0.04 to a nearly flat distribution (fitted solid black line) with the value of ~0.05 at 1 Hz. *G*, half-time to activation ($t_{1/2}$)from quiescent state (solid grey circles, n~5–10 cells) is plotted against frequency, which reach a plateau of 2 s by 0.5 Hz. Error bars indicate SEM. The fitted line (solid black) to the data demonstrates this trend.

equation with a Hill coefficient value of $n = 3.8$ and $K_D = 300$ nM. The departure of the Hill coefficient from 6 (as would be predicted for the expected 6 calcium ions required for full activation) implies a high level of cooperativity between the 6 calcium binding sites. The Hill coefficient of 3.8 (implicating four Ca^{2+} ions required for activation) is quantitatively consistent with previous *in vitro* biochemical assays measuring the dependence of calcineurin phosphatase activity on calcium concentration (Stemmer & Klee, 1994), where strong cooperativity and a Hill coefficient of 3 were observed. Assuming that the Hill coefficients (n) are roughly the same for both activation (our assay) and activity (Stemmer and Klee) measurements, an algebraic manipulation implies that under the steady-state assumption, the activation assayed by our FRET sensors should be related to the *in vitro* calcineurin phosphatase activity by the following relation:

$$Activity = \frac{1}{1 + \frac{FR_{Norm}}{1 - FR_{Norm}} \left(\frac{K_{D,activity}}{K_{D,activation}} \right)^n} \quad (1)$$

where $K_{D,activity}$ and $K_{D,activation}$ denote the calcium concentration required for half-maximal activity and conformational activation of calcineurin, respectively.

Coupling conformational FRET activation of the calcineurin sensors to NFAT nuclear translocation

DuoCaN and UniCaN are sensors of the conformational activation state of calcineurin, similar to the widely used CaMKII sensor Camuiα (Takao *et al.* 2005; Erickson *et al.*, 2011). We showed that under steady-steady conditions the activation might be related to biochemically measured activity (eqn (1)). However, this activation state may not be directly related to the dynamic phosphatase activity of calcineurin in live cells. We therefore employed NFAT translocation as a read-out of calcineurin activity to correlate calcineurin function with sensor activation. The specific fluorescent proteins employed within the sensors (Cer and Ven) allowed for measurement of mCherry-tagged NFAT in the presence of the sensor.

Adding thapsigargin to HEK cells again causes a rise in $[Ca^{2+}]_i$ that activates calcineurin, resulting in NFAT translocation into the cell nucleus. Exemplar time-lapse images of mCherry-NFAT translocation into the nucleus are shown following the application of 1 μM thapsigargin at time 0 (Fig. 4*A* DuoCaN, Fig. 4*F* UniCaN). The fluorescent signals from the FRET (green) and CFP (blue) channels are shown in Fig. 4*B* (DuoCaN) and Fig. 4*G* (UniCaN), demonstrating the homogenous expression of the sensor within the cytosol. NFATc1 nuclear translocation was quantified by computing the ratio of nuclear red fluorescence to the whole-cell red fluorescence, $F_{nuc} = \frac{mCherry_{nuclear}}{mCherry_{total}}$ (Fig. 4*C* for DuoCaN and Fig. 4*H* for UniCaN). The sensor response was simultaneously quantified by computing the normalized change in $R = \frac{FRET}{CFP}$ such that $\bar{R}_{sensor} - 1 = (R/R_0 - 1)$. Figure 4*D* illustrates the transient activation of DuoCaN, while Fig. 4I shows the corresponding UniCaN response. The results indicate that a short transient (~2.5 min) of calcineurin activation is sufficient for complete NFAT nuclear import (Fig. 4*C*, *D*, *H*, *I*). While the sensor activation transient declines to near basal levels after ~2.5 min, the fraction of nuclear NFAT continues to rise. This nuclear NFAT fraction reaches a steady-state level after 9 min. These observations are consistent with mathematical modelling of NFAT dynamics demonstrating that a high level of cooperativity between the 13 serine residues of NFAT can lead to a switch-like behaviour in NFAT activation dynamics (Salazar & Hofer, 2003, 2009).

The change in nuclear NFAT fraction at the plateau, $\Delta F_{nuc} = F_{nuc,\infty} - F_{nuc,0}$, was correlated with the area under the curve of the sensor response ($Q_s = \int (1 - \frac{R}{R_0}) dt = \int (1 - \bar{R}_{sensor}) dt$) as shown in Fig. 4*E* and *J*. Each

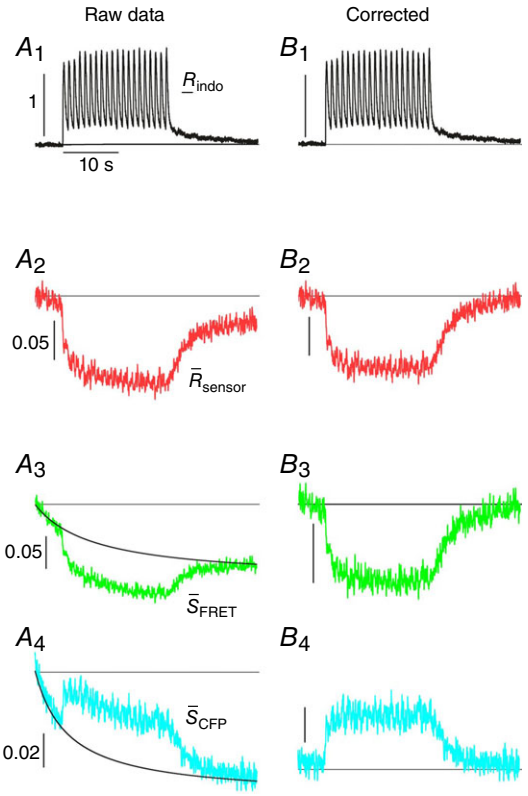

Figure 6. Representative raw data before and after correction of photobleaching
A, $\bar{R}_{sensor}$, the raw traces for FRET (green) and CFP (blue) signals for DuoCaN in NRVMs paced at 1 Hz. The fit for photobleach correction is shown as a black curve (A_3, $_4$). *B*, the same data as in *A*, with the photobleaching artifact removed. Note that the ratio of the FRET to CFP signals largely corrects for the bleaching observed in individual channels (A_2 *vs.* B_2).

point in Fig. 4*E* and *J* corresponds to a single cell. Both DuoCaN and UniCaN population data were fitted with single exponential functions,

$$\Delta F_n = A\left(1 - e^{-\frac{Q_s}{c}}\right) \quad (2)$$

with $c = 9$, and $A = 0.42$ for DuoCaN and $A = 0.45$ for UniCaN. In fact, eqn(2) is the solution of the following differential equation for $F_n(t)$:

$$\frac{dF_n}{dt} = \left(\frac{1}{c}\right)\left(1 - \bar{R}_{\text{sensor}}(t)\right)(F_{\text{tot}} - F_{\text{n}}) = k_{\text{in}}(t)(F_{\text{tot}} - F_{\text{n}}) \quad (3)$$

where $k_{\text{in}}(t)$ is the rate constant for fractional NFAT nuclear accumulation as shown in Fig. 4*A* and F.

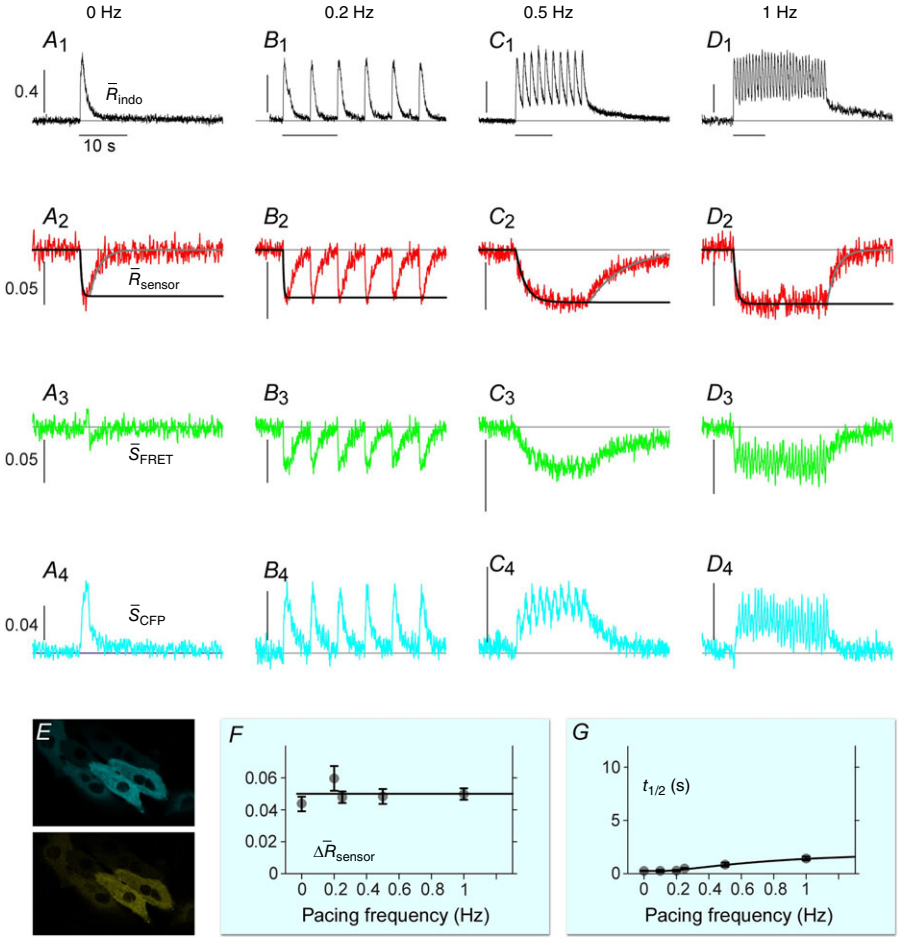

Figure 7. UniCaN activation responding to electrical stimulations in NRVMs
A–D, indo-1 and UniCaN responses for an exemplar cell.*A*, single stimulation pulse elicits a strong calcium transient (A_1, black). $\bar{R}_{\text{sensor}}$ decreases with the rise of $[Ca^{2+}]$ (A_2, red). The trend-lines to the activation (solid black) and inactivation portions (solid grey) are shown. FRET signal (A_3, S_{FRET}, green) decreases, while the CFP signal increases (A_4, S_{CFP}, cyan). Scale bars indicate the normalized change of each signal. *B*, pacing at 0.2 Hz elicits calcium transients (B_1, black)that activate the sensor (B_2, red trace), with a simultaneous decrease in FRET signal (B_3, green) and increase in CFP channel (B_4, cyan). *C*, pacing at 0.5 Hz with a duration of 20 s following a 10 s silent period (C_1) activates the sensor (C_2, red). Individual FRET and CFP channels are shown (C_3 and C_4, respectively). Motion artifacts are present in the CFP signals (C_4), but not in the ratio of the two (C_2). *D*, following a 10 s silent period, pacing at 1 Hz for 30 s produces large calcium transients (D_1, black) that activate the sensor (D_2, red with fitted line to activation and inactivation shown in solid black and grey lines). Simultaneous decrease in FRET signals (D_3, red) and increase in CFP signals (D_4, cyan) are shown. Strong contraction-induced motion artifacts are present in the individual FRET and CFP channels that are corrected for in the ratio of the two in D_2. *E*, UniCaN expression and cellular distribution in NRVMs, shown by imaging through CFP channel (top, cyan) and FRET (bottom, yellow) indicating a diffuse cytoplasmic distribution. *F*, population data of normalized amplitude is plotted against simulation frequencies (solid grey circles with error bars indicating SEM, n~5–10 cells), demonstrating a nearly flat distribution (solid black line fit). *G*, half-time to activation ($t_{1/2}$)from quiescent state is plotted versus frequency (solid grey with error bars shown in black, n~5-10 cells) indicating a slow increase to a 2 s value at 1 Hz. The trend-line (solid black) is also drawn.

Equation(3) implies that $k_{in}(t) = (\frac{1}{c})(1 - \bar{R}_{sensor}(t))$. This relationship implies that the normalized sensor output is linearly related to the rate of NFAT nuclear import. In other words, this argues that the conformational activation observed by the sensors is linearly related to the activity assayed by the rate of NFAT nuclear import. Thus, the normalized sensor output ($-\Delta R/R_0$) is not only a measure of conformational activation, but also of calcineurin activity.

DuoCaN and UniCaN deployment in NRVMs

Given the remarkable response of DuoCaN and UniCaN in HEK293 cells, the sensors were deployed in primary

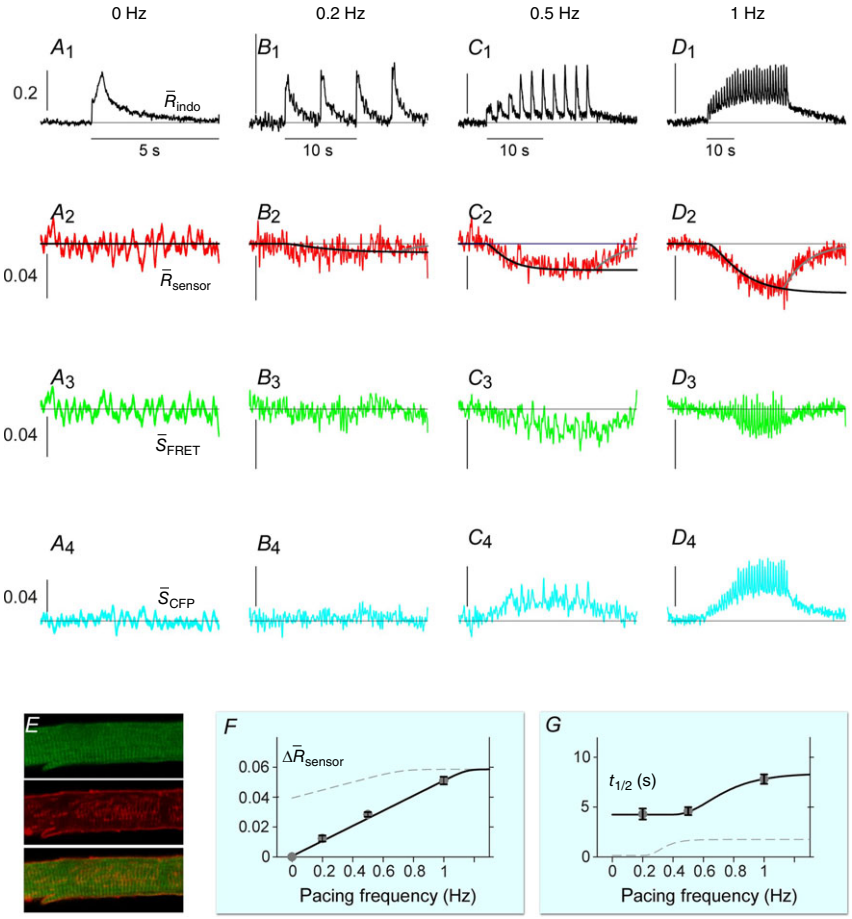

Figure 8. DuoCaN activation in response to field stimulation in aGPVMs
A–D, indo-1 and DuoCaN sensor signals from an exemplar cell are shown. *A*, a single pulse elicits a calcium transient (A_1, black). The sensor is not activated and $\bar{R}_{sensor}$ remains at the baseline (A_2, red). Scale bar indicates normalized change of the signal throughout. Normalized CFP (A_2) and FRET (A_3) channels are silent. *B*, stimulation at 0.2 Hz results in calcium transients in the cell (B_1). The corresponding sensor response is shown (B_2) illustrating a small decrease (~0.005); the fit to activation (solid black) and inactivation (solid grey) is indicated. Individual FRET (B_3) and CFP (B_4) channel signals are shown with the change largely masked by motion artifacts. *C*, a 0.5 Hz stimulation train elicits calcium transients gradually increasing in amplitude, with upward shifting baseline indicating calcium summation (C_1). This in turn activates the sensor as is apparent from the change in *FR* (C_2). Corresponding FRET (C_3) and CFP (C_4) channels are also shown. *D*, pacing at 1 Hz for 30 s leads to a robust increase in sensor activation (D_2) with subsequent decline to the basal level after the pacing was turned off. Individual FRET (D_3) and CFP (D_4) channels are shown. Strong motion artifacts are present in each individual signal and disappear in $\bar{R}_{sensor}$ (D_2). *E*, DuoCaN sensor expression and distribution in aGPVMs evaluated by imaging through CFP channel (green) and di-4-ANEPPS (red). The sensor is located in the vicinity of T-tubules, as demonstrated by the overlay of the two channels (bottom). *F*, population data of sensor activation versus stimulation frequencies are plotted (grey filled circles and solid black line for the trend-line, average of $n = 4$–10 cells for each point). The sensor activation shows a gradual rise in amplitude as the pacing rate is increased. The aGPVMs are contrasted with the corresponding nearly flat NRVM trend-line (dashed-grey). *G*, the half-time to activation from quiescent state in aGPVMs is around 5 s at 0.5 Hz and 10 s at 1 Hz (black filled circles and black line), which is about 5 times slower than that of NRVMs (dashed grey line).

cells equipped with native calcium cycling activity. NRVMs were chosen as a widely used model system featuring robust calcium transients in response to electric field stimulation in culture. Expression of either sensor demonstrated a nearly uniform cytoplasmic distribution (Fig. 5*E* for DuoCaN and Fig. 5*E* for UniCaN). No apparent toxicity was observed for the first 24 h of continuous expression.

Figure 5*A* illustrates the behaviour of DuoCaN in an exemplar NRVM. A single stimulation pulse elicited a strong calcium transient with a duration of ∼3 s as reported by the indo-1 calcium dye (Fig. 5A_1). Accordingly, the normalized FRET signal first decreased and then returned to the basal level (Fig. 5A_3) and the normalized CFP signal first increased and then returned to baseline (Fig. 5A_4). The ratio of these two signals was used as a read out of sensor activation (Fig. 5A_2). During 0.2 Hz stimulation (Fig. 5*B*), DuoCaN responded with off kinetics of ∼5 s. However, faster pacing resulted in a cumulative effect on calcineurin activation (Fig. 5*C*, *D*). To better quantify the on and off kinetics of the sensor, recordings included an unstimulated baseline prior to pacing, as well as a prolonged post-pacing interval, allowing return of the sensor signal to the baseline following the cessation of stimulation. This baseline signal also allowed for straightforward correction of the photobleaching effect shown in the raw traces (Fig. 6). This accumulation of calcineurin activation is demonstrated by 0.5 Hz pacing of the cell in Fig. 5*C*. The sensor response reached a steady-state value after about 13 s. Tetanus stimulation at 1 Hz (Fig. 5*D*) resulted in similar accumulation of sensor activation, demonstrating a clear plateau in sensor response. The population data for $\bar{R}_{\text{sensor}}$ versus frequency is shown in Fig. 5*F*, demonstrating that the sensor activation reaches a maximum level of 0.06 with 1 Hz pacing. The population data for half-time to activation from a quiescent state ($t_{1/2}$) are plotted against frequency in Fig. 5*G*. This value reaches a maximum of 2 s by 0.5 Hz pacing frequency (Fig. 5*G*).

UniCaN behaves similarly when deployed in NRVMs. It responds transiently to a single stimulus pulse with accumulated activation observed at pacing frequencies of 0.5 Hz or higher (Fig. 7*A*–*D*). Interestingly, the maximum capacity of UniCaN activation (∼0.05, Fig. 7*F*) is quite similar to that of DuoCaN (∼0.06, Fig. 5*F*). On the other hand, the $t_{1/2}$ as a function of frequency demonstrates a slower rise as compared to DuoCaN (Fig. 7*G* versus Fig. 5*G*). This could be due to the existence of a non-cleavable linker between the two subunits in UniCaN,

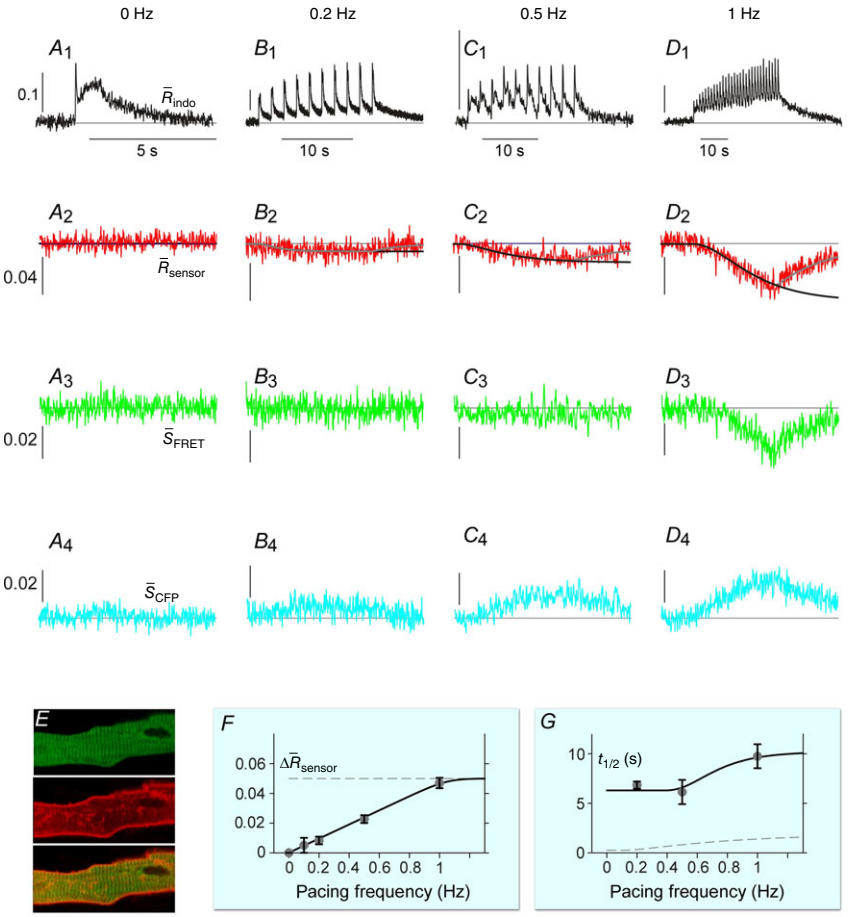

Figure 9. UniCaN activation in response to field stimulations in aGPVMs
A–D, indo-1 and DuoCaN sensor activation for an exemplar cell.*A*, a single pulse of calcium (A_1) does not induce any change in *FR* (A_2). Individual CFP (A_3) and FRET (A_4) signals are shown and remain at the baseline for the duration of the calcium pulse. Scale bars indicate the fractional response of each signal. *B*, pacing at 0.2 Hz (B_1) elicits modest activation (∼0.01) in *FR* (B_2). FRET and CFP channel signals are shown in B_3 and B_4. *C*, 0.5 Hz stimulation for 20 s results in cumulative sensor activation (C_2). *D*, pacing at 1 Hz for 50 s leads to a robust increase in sensor activation (D_2, fit of the activation state is shown by solid black line, fit of the inactivation state is indicated by solid grey line). *E*, UniCaN sensor distribution in aGPVMs is approximately t-tubular. CFP (green) and di-4-ANEPPS (red) channels are shown along with an overlay of the two channels (bottom). *F*, population aggregate amplitude versus simulation frequency for aGPVMs (grey filled circles with solid black line fit, error bars indicate SEM (n ∼ 4–10 cells for each point). The sensor activation shows a gradual rise in amplitude (solid black line). In contrast, the corresponding NRVM curve (dashed grey line) is flat at around ∼0.05. *G*, the population data for half-time to activation in aGPVMs is shown (grey filled circles and black trend-line). This is contrasted with the NRVM curve (dashed grey),which exhibits much faster kinetics.

which might slow down the response of the sensor due to steric hindrance.

Calcineurin activation dynamics in aGPVMs

We next deployed the sensors in acutely isolated aGPVMs,which are functionally more comparable to adult human ventricular myocytes than are NRVMs. aGPVMs possess all the major cellular structures and signalling pathways required for mature myocyte function. However, compared to NRVMs, aGPVMs have higher background fluorescence and are more resistant to DNA transfection, making them a challenging cell type for FRET-based sensor studies. Gratifyingly, adenoviral-mediated expression of DuoCaN and UniCaN in aGPVMs was efficient and caused no appreciable cell toxicity within 36 h. Strong z-line targeting of the sensors was observed as indicated by co-imaging with the membrane-localized dye di-4-ANNEPS (Fig. 8*E* for DuoCaN and Fig. 9*E* for UniCaN), consistent with the previously described localization pattern of calcineurin in cardiomyocytes (Santana *et al.* 2002).

Both DuoCaN and UniCaN displayed a functional response in aGPVMs that was distinctly different from their responses in NRVMs. In aGPVMs, the calcium transient elicited by a single electrical stimulus failed to activate the sensor (Fig. 8*A*). A train of electrical stimuli at 0.2 Hz also induced only slight activation of either DuoCaN (Fig. 8B_2) or UniCaN (Fig. 9B_2) despite a large change in Ca^{2+} signal (Figs 8B_1 and 9B_1). A significant sensor response was only seen upon increasing the pacing rate to 0.5 Hz (Figs 8*C* and 9*C*). Under this condition, a cumulative sensor response was observed for both DuoCaN (Fig. 8*C*) and UniCaN (Fig. 9*C*). Notably, as in NRVMs, DuoCaN appeared to respond faster than UniCaN, reaching a clear plateau in activation. Stronger activation was observed with 1 Hz pacing, with DuoCaN again reaching a plateau (Fig. 8D_2) faster than the UniCaN sensor (Fig. 9D_2). Both the FRET (Fig. 8D_3) and the CFP (Fig. 8D_4) signals displayed strong amplitude fluctuations due to mechanical contractions of the myocyte. These large motion artifacts were compensated for in the $\bar{R}_{sensor}$ signal (Fig. 8D_2). Thus, ratiometric sensors such as DuoCaN and UniCaN circumvent the need for the application of contraction blocking agents that could interfere with the normal calcium cycling processes of the cell. Altogether, DuoCaN and UniCaN have demonstrated robust signals in a useful and often challenging system.

The maximal amplitude of the sensor responses is similar in both NRVMs and in aGPVMs, as demonstrated by plotting the amplitude of the sensor response versus frequency. Both DuoCaN (Fig. 8*F*) and UniCaN (Fig. 9*F*) exhibit larger responses in amplitude as frequency increases, and their responses appear to plateau near the same values as in NRVMs (dashed line). The slope of the frequency-dependent rise in amplitude, however, is more steeply dependent on frequency in aGPVMs as compared to NRVMs, indicating a requirement for cumulative recruitment of calcineurin in adult myocytes. This is in contrast to responses in NRVMs where both sensors responded effectively to single pulses (Figs 5*A* and 7*A*).

In addition to the difference in the frequency dependence of the sensor responses, there is also a major difference in the time course of sensor activation in aGPVMs as compared to NRVMs. Plotting $t_{1/2}$ as a function of frequency for DuoCaN (Fig. 8*G*) or UniCaN (Fig. 9*G*) deployed in aGPVMs demonstrates a stark contrast with the same data from NRVMs (dashed line). The time constant for DuoCaN activation is 2.5-fold slower at 0.5 Hz pacing and 4-fold slower in response to 1 Hz pacing in aGPVMs than in NRVMs. A similar pattern is seen for UniCaN. As compared to NRVMs, a clear slowing of sensor activation can be seen. This difference in sensor activation kinetics in aGPVMs versus NRVMs hints at distinct mechanisms for calcineurin activation within the different milieu of the two cell types. Such dissimilarity within the two cell types is not unexpected given the localization pattern of calcineurin in aGPVMs, reinforcing this model system as a functional correlate to human ventricular myocytes.

Mathematical modelling of calcineurin sensor response in cardiomyocytes

The DuoCaN and UniCaN sensors provide a window into the dynamics of calcineurin activation in primary cardiomyocytes and offer the possibility of accurate estimation of important kinetic parameters for calcineurin activation in live cells. We thus utilized our myocyte data to constrain a kinetic model of calcineurin activation, allowing extrapolation of the binding rates for Ca^{2+} and Ca^{2+}/CaM to the calcineurin complex. These parameters can be used to predict the activity of calcineurin in response to given calcium signals in diverse biological systems. The goal is thus to determine a single set of values for the dissociation constant of Ca^{2+}/CaM from calcineurin, $K_{D,CnA}$, and the dissociation rate of the same reaction, $k_{off,CnA}$, capable of fitting both the NRVM and the aGPVM DuoCaN data. Note that DuoCaN is chosen for this model over the UniCaN sensor because it is expected to more closely approximate the native conformation of calcineurin. To begin, a simplified kinetic model was constructed based on a previous model of calcineurin dynamics in the heart (Saucerman & Bers, 2008) (see Methods for details). The DuoCaN sensor data were fitted with the assumption that the normalized fractional sensor response is proportional to the fraction of calcineurin in the full and partially active state (Ca_4CaMCa_4CN and Ca_4N, respectively) such that:

$$-\bar{R}_{\text{sensor}} = -\frac{\Delta R}{R_0}(t) = \alpha\,[\text{Ca}_4\text{CN}] + \beta[\text{Ca}_4\text{CaMCa}_4\text{CN}] \quad (4)$$

where α and β are constants.Values for the binding of two Ca^{2+} ions to CaNB were set initially as $K_{D,CnB} = 0.5\ \mu M$ and $k_{off,CnB} = 1\ s^{-1}$ as reported based on steady-state biochemical assays (Saucerman & Bers, 2008). The parameters for Ca^{2+}/CaM binding to CaNA were determined by fitting the model to the experimental data as follows.The calcium transients obtained with the indo-1 dye (Fig. 10*A* black) were converted to true calcium concentrations and used as the system input allowing the model to be fit to the corresponding DuoCaN sensor data (Fig. 10*A* red). Fitting this model to the DuoCaN data obtained in an NRVM paced at 0.1 Hz (Fig. 10*B* black, note $1-\bar{R}_{\text{sensor}}$ values are used for the fit) generates a predicted calcineurin response (red). The fit was obtained with the values $K_{D,CnA} = 100$ pM, and $k_{off,CnA} = 1\ s^{-1}$ for Ca^{2+}/CaM binding to CaNA. Compared to the previously used value in a mathematical model (Saucerman & Bers, 2008), k_{off} is 3 orders of magnitude faster, while the predicted K_D for the same binding reaction is ∼3-fold larger. The same model could be fitted to sensor data from variable pacing frequencies in both NRVMs and aGPVMs (exemplars shown in Fig. 10*C*, *D*), accurately predicting the sensor activation in the myocytes in response to multiple Ca^{2+} inputs. Remarkably, this model is capable of capturing both the activation and the inactivation trajectories of DuoCaN dynamics in NRVMs and aGPVMs. A single set of $K_{D,CnA}$ and $k_{off,CnA}$ values (Fig. 10*E*) fitted the data in both NRVMs and aGPVMs, increasing our confidence in this result.

Careful inspection of the model inspired an interesting prediction for the parameter C_1 (available free CaM in the system according to eqn (1)). As demonstrated in Fig. 10*F*, increasing C_1 modulates the plateau amplitude of calcineurin activation for a given calcium train profile in aGPVMs. The steady-state activation value is almost doubled (to ∼0.1, blue trace) as C_1 is increased from the fitted value of 30 nM (0.05, red trace) to 75 nM (blue trace). The steady-state value of activation is further increased as C_1 is raised to 95 nM (∼0.2, green trace). In all, mathematical modelling combined with quantitative FRET measurements not only provided a method for determining the kinetic parameters of Ca^{2+} and Ca^{2+}/CaM binding to calcineurin, but also generated an interesting hypothesis for how calcineurin could be modulated by other proteins (such as CaM) in various environments.

Discussion

The calcineurin reporters developed here showcase a 40% change in *FR* (Fig. 2A_2, B_2) in response to thapsigargin-induced calcium release from the intracellular calcium stores, and a 100% change in response to an excess calcium load following ionomycin treatment in HEK293 cells overexpressing CaM (Fig. 3). The suitable dynamic range and magnitude of response of these sensors were demonstrated by clear readouts of the time-dependent activation of calcineurin in neonatal and adult cardiomyocytes. These sensors substantially expand the repertoire of tools available to assay calcineurin–NFAT dynamics. In particular, they have a large dynamic range and more closely resemble endogenous calcineurin as compared to previously reported sensors (Newman & Zhang, 2008; Mehta *et al.* 2014). DuoCaN and UniCaN are the first to successfully capture dynamic calcineurin responses in primary cells. Deployment of the sensors in various cell types and tissues thus promises new insight into calcineurin signalling in numerous biological systems.

Differential calcineurin activation in neonatal and adult cardiomyocytes

Calcineurin readily activates in response to single calcium pulses in NRVMs, while in aGPVMs calcineurin seems to only activate at pacing frequencies that result in calcium accumulation from one pulse to the next. At higher frequencies, calcineurin activation is cumulative and follows the corresponding calcium train. Thus, the rapid heart rate of neonatal rats (∼320 b.p.m.) and human fetal myocytes (120–200 b.p.m.) may drive some level of continuous calcineurin activation leading to nuclear localization of NFAT (Fig. 11*A*). This type of activity would be in agreement with the known role of the calcineurin/NFAT pathway in cardiac development (de la Pompa *et al.* 1998; Ranger *et al.* 1998; Schulz & Yutzey, 2004). Furthermore, this is also consistent with studies showing that NFAT is localized to the nucleus in 12% of NRVMs in quiescent culture conditions (MacDonnell *et al.* 2009). Adult myocytes appear to have a remarkably different pattern of calcineurin activity. In aGPVMs, calcineurin seems to respond only when there is a rise in basal calcium from one beat to the next. Thus, in human myocytes, where there is no beat-to-beat accumulation of calcium under normal conditions (Piacentino *et al.* 2003), calcineurin is likely to remain inactive under healthy conditions, consistent with the finding that calcineurin activation in adult myocytes would be pathologically hypertrophic (Sussman *et al.* 1998; Wilkins *et al.* 2004; van Berlo *et al.* 2013). The cumulative activation of calcineurin (Figs 8 and 9) would predict nuclear localization of NFAT in adult myocytes. Such frequency-dependent localization of NFAT has indeed been shown in adult feline myocytes in culture, where increasing amounts of NFAT localization at faster pacing rates occurred (MacDonnell *et al.* 2009). It is reassuring that such a frequency-dependent increase in NFAT translocation agrees with the frequency dependence

of calcineurin activation in aGPVMs observed with both DuoCaN and UniCaN sensors (Figs 8*F* and 9*F*). In another study, the NFATc1 (but not NFATc3) isoform was shown to be localized to the nucleus under resting conditions in both atrial and ventricular myocytes and NFATc1 nuclear localization was reduced by inhibiting calcineurin (Rinne *et al.* 2010). This finding substantially adds to the complexity of the mechanisms involved in the transduction of the signals from calcineurin to different isoforms of NFAT, and necessitates the need for tools such as DuoCaN and UniCaN to help unravel the mechanisms underlying the precise control of Cn-NFAT signalling in cardiomyocytes.

It appears that there is a significant difference in neonatal versus adult myocyte calcineurin activation and NFAT localization. As we are able to describe both NRVM and aGPVM data with a single mechanistic kinetic model, we expect that this differential activation does not arise from fundamental differences in the pathways for calcineurin activation (Fig. 11*A*). It is thus

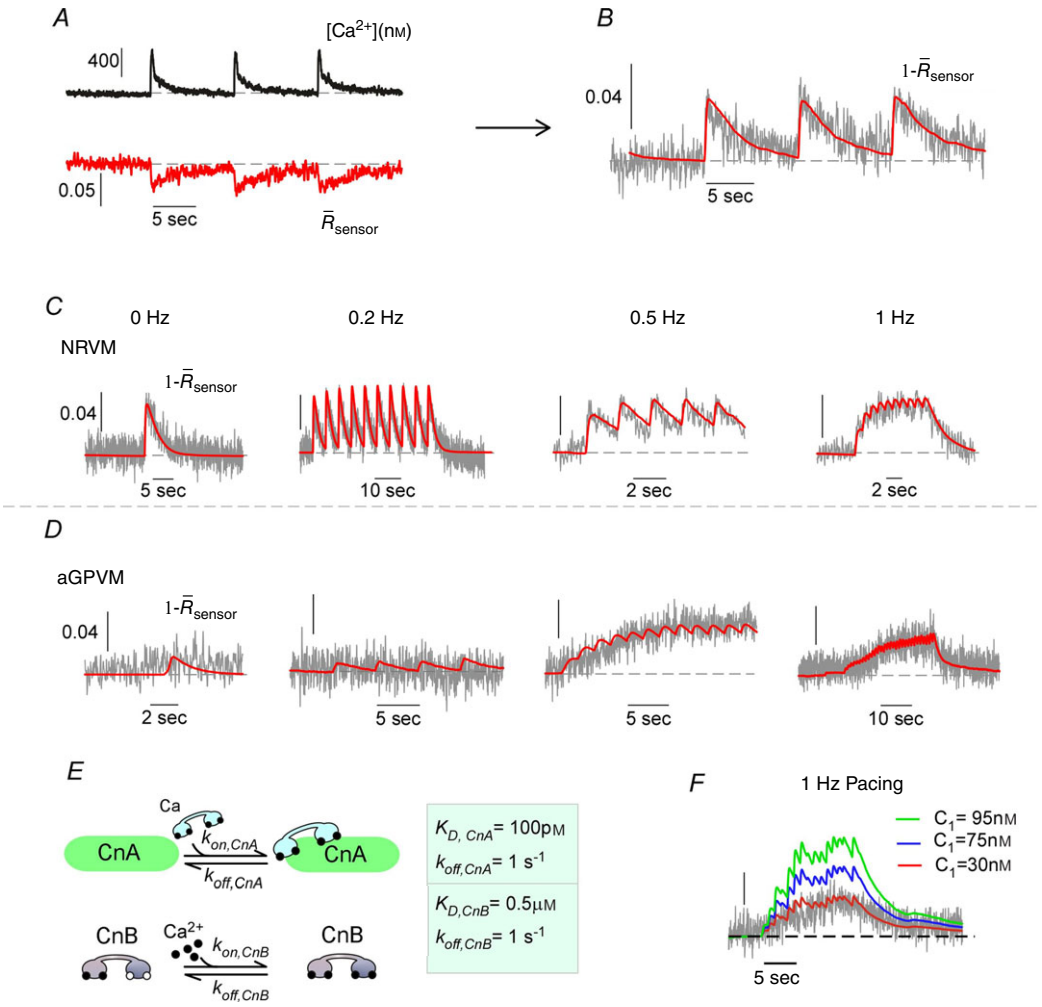

Figure 10. Mathematical modelling of calcineurin sensor response in cardiomyocytes
A, experimental measurements of indo-1 signal (top,black) and the corresponding DuoCaN sensor activation response (bottom, red) in an NRVM cell paced at 0.1 Hz, describing the empirical input to the model. *B*, indo-1 signal is converted to $[Ca^{2+}]$ concentration and interpolated, serving as an input to the kinetic model. The numerical solutions of the kinetic model (solid red lines) are fitted to the recorded fractional sensor activation ($1 - \bar{R}_{sensor}$, black traces) by eqn (4).*C*, model fits (red) to calcineurin activation (grey) in NRVM cells for a single pulse (the fitted value of $C_1 = 30$ nM), 0.2 Hz pacing ($C_1 = 40$ nM), 0.5 Hz pacing ($C_1 = 120$ nM) and 1 Hz pacing ($C_1 = 70$ nM).*D*, model fit to calcineurin activation in aGPVMs for single pulse (the fitted value of $C_1 = 30$ nM), 0.2 Hz pacing ($C_1 = 30$ nM), 0.5 Hz pacing ($C_1 = 70$ nM) and 1 Hz pacing ($C_1 = 100$ nM). *E*,summary of the important binding parameters for Ca^{2+}/CaM binding to calcineurin ($K_{D,CnA} = 100$ pM and $k_{off,CnA} = 1\ s^{-1}$, top cartoon) and Ca^{2+} binding to the B subunit of calcineurin ($K_{D,CnB} = 0.5\ \mu M$, $k_{off,CnB} = 1\ s^{-1}$, bottom cartoon) estimated by the fit to 25 NRVMs and 10 aGPVMs at different frequencies. *F*,the kinetic model is fitted to an aGPVM cell paced at 1 Hz (red, $C_1 = 30$ nM). The same calcium transient was used as input but C_1 was varied. Two different curves are shown for $C_1 = 75$ nM (blue) and $C_1 = 95$ nM (green) indicating modulation of the sensor activation with C_1.

tempting to speculate that some of the differences in calcineurin activity between neonatal and adult myocytes may arise from the contrasting calcineurin localization pattern within these cells. In NRVMs both DuoCaN and UniCaN were homogeneous throughout the cytosol (Figs 5*E* and7*E*), indicating a similar pattern for native calcineurin. In aGPVMs, on the other hand, a t-tubular localization pattern was seen (Figs 8*E* and 9*E*). As dyadic calcium levels are expected to be greater than the cytoplasmic concentration (Despa *et al.* 2014), the reduced response of calcineurin in adult cells cannot result from a simple difference in calcium input. One possibility is that lower calcineurin activity in adult myocytes is partially due to co-localization of calcineurin near endogenous inhibitors such as AKAP79 (Li *et al.* 2012) and CaMKII (MacDonnell *et al.* 2009). In addition, differences in the amount of available local CaM may be involved, as follows. The maximum calcineurin activation in both NRVMs (Figs 5*F* and 7*F*) and aGPVMs (Figs 8*F* and 9*F*) was significantly lower than in HEK cells (Fig. 2A_2, B_2), indicating that there may be a limiting reagent in the activation pathway. As both A and B subunits of calcineurin are overexpressed and a large Ca^{2+} transient was directly measured, CaM becomes the most likely candidate. Adjusting CaM concentrations in the kinetic model of calcineurin activation supports such a supposition. Increasing the amount of free CaM in the model enhanced the maximum level of calcineurin activation (Fig. 10*F*). Applying this idea to NRVMs, CaM may be readily accessible to calcineurin in the cytosol, but at a lower free concentration as compared to HEK cells. In aGPVMs, dyadic localization may position calcineurin in an area with relatively lower levels of free CaM, an effect that may be amplified by decreased CaM expression due to culture conditions (Maier *et al.* 2006). While this is not known, recent observations show that CaM in adult myocytes is strongly buffered by ryanodine receptors that are in this dyadic region (Yang *et al.* 2014). The use of a FRET-based sensor of CaM was also shown to respond only in the presence of overexpressed CaM in cultured myocytes, further reinforcing the CaM availability hypothesis (Maier *et al.* 2006). Finally, this idea is also supported by a recent study that utilized a sensor of calcineurin to show that variations in subcellular CaM distribution can modulate the spatial and temporal dynamics of the calcineurin response (Mehta *et al.* 2014).

The differences in calcineurin activity between neonatal and adult myocytes may point to a common mechanism between developing and failing hearts. While calcineurin-driven NFAT translocation to the nucleus (Fig. 11*A*) is known to promote pathological adult cardiac hypertrophy (Molkentin *et al.* 1998; Wilkins *et al.* 2004), constitutive activation of calcineurin might be necessary for the normal maturational hypertrophy of a developing myocyte (Fig. 11*B*). Once the myocyte has matured, calcineurin activity would be reduced under normal physiological conditions. However, perturbations in calcium handling processes (Muth *et al.* 2001), altered levels of CaM (Gruver *et al.* 1993) and a myriad of other changes in the failing heart may lead to pathological

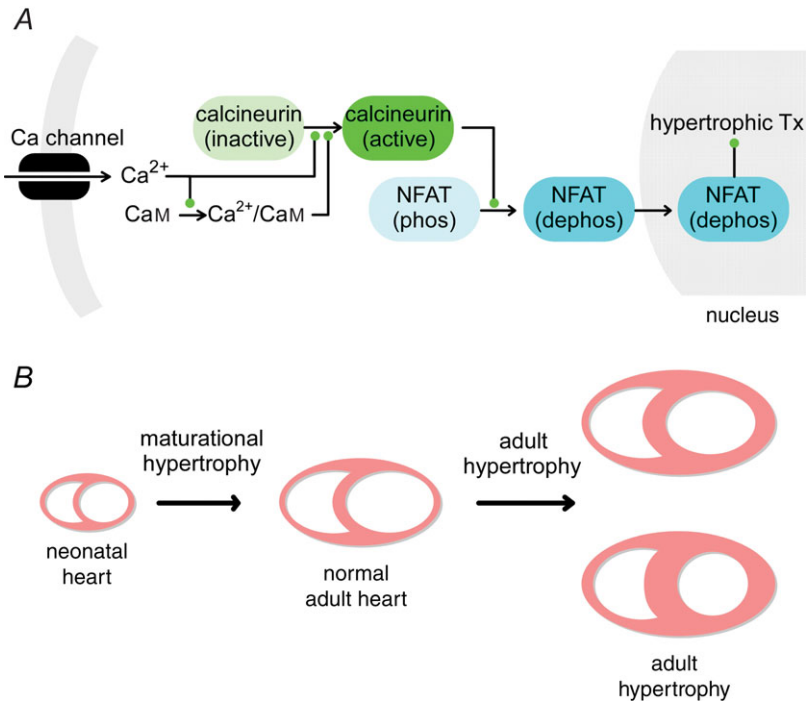

Figure 11. Maturation and adult hypertrophy and calcineurin dynamics
A, Ca^{2+} influx from Ca^{2+} channels activates CaM, which in turn binds and activates the calcineurin complex. This results in NFAT translocation to the nucleus and may induce a hypertrophic signal. *B*, in the neonatal heart, the kinetics of calcineurin activation is fast so that calcineurin is prone to be activated, possibly resulting in the activation of maturational hypertrophic genes. In the adult heart, calcineurin activation is expected to be low under normal conditions, but circumstances causing pathological activation of the pathway may lead to adult cardiac hypertrophy.

activation of the calcineurin/NFAT pathway, resulting in hypertrophy of the adult heart (Fig. 11*B*).

Future applications of the calcineurin sensors

Our results with DuoCaN and UniCaN provide support for the idea that FRET-based sensors can be exceptional tools for understanding normal and pathological signalling in biological systems. The two sensors could be used to test the aforementioned hypothesis that calcineurin may be highly active in failing hearts, providing new insight into cardiac pathophysiology. In addition, the sharp dependence of the model on levels of CaM makes the potential effect of recently discovered CaM mutations (Crotti *et al.* 2013; Limpitikul *et al.* 2014) on calcineurin dynamics an exciting new realm of inquiry. In addition, the sensors could be utilized to develop new targeted inhibitors of calcineurin that might exhibit lower liver and neurological toxicity (Palmer & Toto, 1991; Burdmann *et al.* 2003). Finally, given the robust response of the sensors in aGPVMs, a high probability of *in vivo* functionality is expected. Thus, the development of transgenic animals expressing DuoCaN or UniCaN looms as an exciting possibility. The unimolecular nature of UniCaN would allow subcellular targeting, adding a new dimension to the applicability of this sensor. In all, both DuoCaN and UniCaN stand as valuable new tools with which to probe calcineurin dynamics in a myriad of biological settings.

References

Alseikhan BA, DeMaria CD, Colecraft HM&Yue DT (2002). Engineered calmodulins reveal the unexpected eminence of Ca^{2+} channel inactivation in controlling heart excitation. *Proc Natl Acad Sci U S A* **99**, 17185–17190.

Aramburu J, Rao A&Klee CB (2000). Calcineurin: from structure to function. *Curr Top Cell Regul* **36**, 237–295.

Beals CR, Clipstone NA, Ho SN&Crabtree GR (1997). Nuclear localization of NF-ATc by a calcineurin-dependent, cyclosporin-sensitive intramolecular interaction.*Genes Dev* **11**, 824–834.

Burdmann EA, Andoh TF, Yu L&Bennett WM (2003). Cyclosporine nephrotoxicity.*Semin Nephrol* **23**, 465–476.

Chlopcikova S, Psotova J&Miketova P (2001). Neonatal rat cardiomyocytes – a model for the study of morphological, biochemical and electrophysiological characteristics of the heart.*Biomed PapMed FacUniv Palacky Olomouc Czech Repub* **145**, 49–55.

Colecraft HM, Alseikhan B, Takahashi SX, Chaudhuri D, Mittman S, Yegnasubramanian V, Alvania RS, Johns DC, Marban E & Yue DT (2002). Novel functional properties of Ca^{2+} channel beta subunits revealed by their expression in adult rat heart cells. *J Physiol* **541**, 435–452.

Crabtree GR (1989). Contingent genetic regulatory events in T lymphocyte activation.*Science* **243**, 355–361.

Crotti L, Johnson CN, Graf E, DeFerrari GM, Cuneo BF, Ovadia M, Papagiannis J, Feldkamp MD, Rathi SG, Kunic JD, Pedrazzini M, Wieland T, Lichtner P, Beckmann BM, Clark T, Shaffer C, Benson DW, Kaab S, Meitinger T, Strom TM, Chazin WJ, Schwartz PJ&George AL Jr (2013). Calmodulin mutations associated with recurrent cardiac arrest in infants. *Circulation* **127**, 1009–1017.

dela Pompa JL, Timmerman LA, Takimoto H, Yoshida H, Elia AJ, Samper E, Potter J, Wakeham A, Marengere L, Langille BL, Crabtree GR & Mak TW (1998). Role of the NF-ATc transcription factor in morphogenesis of cardiac valves and septum.*Nature* **392**, 182–186.

Despa S, Shui B, Bossuyt J, Lang D, KotlikoffMI&BersDM (2014). Junctional cleft $[Ca^{2+}]_i$ measurements using novel cleft-targeted Ca^{2+} sensors. *Circ Res* **115**, 339–347.

Donnelly ML, Luke G, Mehrotra A, Li X, Hughes LE, Gani D&Ryan MD (2001). Analysis of the aphthovirus 2A/2B polyprotein 'cleavage' mechanism indicates not a proteolytic reaction, but a novel translational effect: a putative ribosomal 'skip'. *J Gen Virol* **82**, 1013–1025.

Durand DB, Shaw JP, Bush MR, Replogle RE, Belagaje R&Crabtree GR (1988). Characterization of antigen receptor response elements within the interleukin-2 enhancer.*Mol Cell Biol* **8**, 1715–1724.

Erickson JR, Patel R, Ferguson A, Bossuyt J& Bers DM(2011) Fluorescence resonance energy transfer-based sensor Camui provides new insight into mechanisms of calcium/calmodulin-dependent protein kinase II activation in intact cardiomyocytes. *Circ Res* **109**, 729–738.

Erickson MG, Alseikhan BA, Peterson BZ&Yue DT (2001). Preassociation of calmodulin with voltage-gated Ca^{2+} channels revealed by FRET in single living cells.*Neuron* **31**, 973–985.

Erickson MG, Liang H, Mori MX&Yue DT (2003). FRET two-hybrid mapping reveals function and location of L-type Ca^{2+} channel CaM preassociation. *Neuron* **39**, 97–107.

Graef IA, Mermelstein PG, Stankunas K, Neilson JR, Deisseroth K, Tsien RW & Crabtree GR (1999). L-type calcium channels and GSK-3 regulate the activity of NF-ATc4 in hippocampal neurons. *Nature* **401**, 703–708.

Graef IA, Wang F, Charron F, Chen L, Neilson J, Tessier-Lavigne M & Crabtree GR (2003). Neurotrophins and netrins require calcineurin/NFAT signaling to stimulate outgrowth of embryonic axons. *Cell* **113**, 657–670.

Gruver CL, DeMayo F, Goldstein MA&Means AR (1993). Targeted developmental overexpression of calmodulin induces proliferative and hypertrophic growth of cardiomyocytes in transgenic mice. *Endocrinology* **133**, 376–388.

Grynkiewicz G, Poenie M&Tsien RY (1985). A new generation of Ca^{2+} indicators with greatly improved fluorescence properties. *J Biol Chem* **260**, 3440–3450.

Hardy S, Kitamura M, Harris-Stansil T, Dai Y & Phipps ML (1997). Construction of adenovirus vectors through Cre-lox recombination. *J Virol* **71**, 1842–1849.

Heit JJ, Apelqvist AA, Gu X, Winslow MM, Neilson JR, Crabtree GR & Kim SK (2006). Calcineurin/NFAT signalling regulates pancreatic beta-cell growth and function. *Nature* **443**, 345–349.

Jain J, McCaffrey PG, Miner Z, Kerppola TK, Lambert JN, Verdine GL, Curran T & Rao A (1993). The T-cell transcription factor NFATp is a substrate for calcineurin and interacts with Fos and Jun. *Nature* **365**, 352–355.

Jares-Erijman EA & Jovin TM (2003). FRET imaging. *Nature Biotechnol* **21**, 1387–1395.

Joshi-Mukherjee R, Dick IE, Liu T, O'Rourke B, Yue DT&Tung L (2013). Structural and functional plasticity in long-term cultures of adult ventricular myocytes.*J Mol Cell Cardiol* **65**, 76–87.

Kao SC, Wu H, Xie J, Chang CP, Ranish JA, Graef IA & Crabtree GR (2009). Calcineurin/NFAT signaling is required for neuregulin-regulated Schwann cell differentiation. *Science* **323**, 651–654.

Kasahara A, Cipolat S, Chen Y, Dorn GW 2nd & Scorrano L (2013). Mitochondrial fusion directs cardiomyocyte differentiation via calcineurin and Notch signaling. *Science* **342**, 734–737.

Kim JH, Lee SR, Li LH, Park HJ, Park JH, Lee KY, Kim MK, Shin BA & Choi SY (2011). High cleavage efficiency of a 2A peptide derived from porcine teschovirus-1 in human cell lines, zebrafish and mice. *PLoS One* **6**, e18556.

Klee CB, Crouch TH & Krinks MH (1979). Calcineurin: a calcium- and calmodulin-binding protein of the nervous system. *Proc Natl Acad Sci USA* **76**, 6270–6273.

Klee CB & Krinks MH (1978). Purification of cyclic 3',5'-nucleotide phosphodiesterase inhibitory protein by affinity chromatography on activator protein coupled to Sepharose. *Biochemistry* **17**, 120–126.

Klee CB, Ren H & Wang X (1998). Regulation of the calmodulin-stimulated protein phosphatase, calcineurin.*J Biol Chem* **273**, 13367–13370.

Li H, Pink MD, Murphy JG, Stein A, Dell'Acqua ML & Hogan PG (2012). Balanced interactions of calcineurin with AKAP79 regulate Ca^{2+}-calcineurin–NFAT signaling. *Nat Struct Mol Biol* **19**, 337–345.

Li H, Rao A & Hogan PG (2011). Interaction of calcineurin with substrates and targeting proteins.*Trends Cell Biol* **21**, 91–103.

Limpitikul WB, Dick IE, Joshi-Mukherjee R, Overgaard MT, George AL Jr & Yue DT (2014). Calmodulin mutations associated with long QT syndrome prevent inactivation of cardiac L-type Ca^{2+} currents and promote proarrhythmic behavior in ventricular myocytes. *J Mol Cell Cardiol* **74**, 115–124.

Liu J, Farmer JD Jr, Lane WS, Friedman J, Weissman I & Schreiber SL (1991). Calcineurin is a common target of cyclophilin-cyclosporin A and FKBP-FK506 complexes. *Cell* **66**, 807–815.

Liu X, Yang PS, Yang W & Yue DT (2010). Enzyme-inhibitor-like tuning of Ca^{2+} channel connectivity with calmodulin.*Nature* **463**, 968–972.

MacDonnell SM, Weisser-Thomas J, Kubo H, Hanscome M, Liu Q, Jaleel N, Berretta R, Chen X, Brown JH, Sabri AK, Molkentin JD & Houser SR (2009). CaMKII negatively regulates calcineurin–NFAT signaling in cardiac myocytes. *Circ Res* **105**, 316–325.

Maier LS, Ziolo MT, Bossuyt J, Persechini A, Mestril R & Bers DM (2006). Dynamic changes in free Ca-calmodulin levels in adult cardiac myocytes.*J Mol Cell Cardiol* **41**, 451–458.

Mehta S, Aye-Han NN, Ganesan A, Oldach L, Gorshkov K & Zhang J (2014). Calmodulin-controlled spatial decoding of oscillatory Ca^{2+} signals by calcineurin. *Elife* **3**, e03765.

Molkentin JD, Lu JR, Antos CL, Markham B, Richardson J, Robbins J, Grant SR & Olson EN (1998). A calcineurin-dependent transcriptional pathway for cardiac hypertrophy.*Cell* **93**, 215–228.

Mondragon A, Griffith EC, Sun L, Xiong F, Armstrong C & Liu JO (1997). Overexpression and purification of human calcineurin alpha from *Escherichia coli* and assessment of catalytic functions of residues surrounding the binuclear metal center.*Biochemistry* **36**, 4934–4942.

Muth JN, Bodi I, Lewis W, Varadi G & Schwartz A (2001). A Ca^{2+}-dependent transgenic model of cardiac hypertrophy: a role for protein kinase Cα. *Circulation* **103**, 140–147.

Newman RH & Zhang J (2008). Visualization of phosphatase activity in living cells with a FRET-based calcineurin activity sensor. *Mol Biosyst* **4**, 496–501.

Palmer BF & Toto RD (1991). Severe neurologic toxicity induced by cyclosporine A in three renal transplant patients. *Am J Kidney Dis* **18**, 116–121.

Piacentino V 3rd, Weber CR, Chen X, Weisser-Thomas J, Margulies KB, Bers DM & Houser SR (2003). Cellular basis of abnormal calcium transients of failing human ventricular myocytes.*Circ Res* **92**, 651–658.

Ranger AM, Grusby MJ, Hodge MR, Gravallese EM, dela Brousse FC, Hoey T, Mickanin C, Baldwin HS & Glimcher LH (1998). The transcription factor NF-ATc is essential for cardiac valve formation. *Nature* **392**, 186–190.

Rinne A, Kapur N, Molkentin JD, Pogwizd SM, Bers DM, Banach K&Blatter LA (2010). Isoform- and tissue-specific regulation of the Ca^{2+}-sensitive transcription factor NFAT in cardiac myocytes and heart failure. *Am J Physiol Heart Circ Physiol* **298**, H2001–H2009.

Robertson BH, Grubman MJ, Weddell GN, Moore DM, Welsh JD, Fischer T, Dowbenko DJ, Yansura DG, Small B & Kleid DG (1985). Nucleotide and amino acid sequence coding for polypeptides of foot-and-mouth disease virus type A12. *J Virol* **54**, 651–660.

Rusnak F & Mertz P (2000). Calcineurin: form and function. *Physiol Rev* **80**, 1483–1521.

Ryan MD, King AM & Thomas GP (1991). Cleavage of foot-and-mouth disease virus polyprotein is mediated by residues located within a 19 amino acid sequence. *J Gen Virol* **72**, 2727–2732.

Salazar C & Hofer T (2003). Allosteric regulation of the transcription factor NFAT1 by multiple phosphorylation sites: a mathematical analysis. *J Mol Biol* **327**, 31–45.

Salazar C & Hofer T (2009). Multisite protein phosphorylation – from molecular mechanisms to kinetic models.*FEBS J* **276**, 3177–3198.

Sanderson JL, Gorski JA, Gibson ES, Lam P, Freund RK, Chick WS & Dell'Acqua ML (2012). AKAP150-anchored calcineurin regulates synaptic plasticity by limiting synaptic incorporation of Ca^{2+}-permeable AMPA receptors. *J Neurosci* **32**, 15036–15052.

Santana LF, Chase EG, Votaw VS, Nelson MT & Greven R (2002). Functional coupling of calcineurin and protein kinase A in mouse ventricular myocytes.*J Physiol* **544**, 57–69.

Saucerman JJ & Bers DM (2008). Calmodulin mediates differential sensitivity of CaMKII and calcineurin to local Ca^{2+} in cardiac myocytes. *Biophys J* **95**, 4597–4612.

Schaeffer PJ, Desantiago J, Yang J, Flagg TP, Kovacs A, Weinheimer CJ, Courtois M, Leone TC, Nichols CG, Bers DM & Kelly DP (2009). Impaired contractile function and calcium handling in hearts of cardiac-specific calcineurin b1-deficient mice. *Am J Physiol Heart Circ Physiol* **297**, H1263–H1273.

Schneider CA, Rasband WS & Eliceiri KW (2012). NIH Image to ImageJ: 25 years of image analysis. *Nat Methods* **9**, 671–675.

Schulz RA & Yutzey KE (2004). Calcineurin signaling and NFAT activation in cardiovascular and skeletal muscle development.*Dev Biol* **266**, 1–16.

Shaner NC, Campbell RE, Steinbach PA, Giepmans BN, Palmer AE & Tsien RY (2004). Improved monomeric red, orange and yellow fluorescent proteins derived from *Discosoma* sp. red fluorescent protein. *Nat Biotechnol* **22**, 1567–1572.

Shaw JP, Utz PJ, Durand DB, Toole JJ, Emmel EA & Crabtree GR (1988). Identification of a putative regulator of early T cell activation genes.*Science* **241**, 202–205.

Stemmer PM & Klee CB (1994). Dual calcium ion regulation of calcineurin by calmodulin and calcineurin B. *Biochemistry* **33**, 6859–6866.

Sun T, Wu XS, Xu J, McNeil BD, Pang ZP, Yang W, Bai L, Qadri S, Molkentin JD, Yue DT & Wu LG (2010). The role of calcium/calmodulin-activated calcineurin in rapid and slow endocytosis at central synapses.*J Neurosci* **30**, 11838–11847.

Sussman MA, Lim HW, Gude N, Taigen T, Olson EN, Robbins J, Colbert MC, Gualberto A, Wieczorek DF & Molkentin JD (1998). Prevention of cardiac hypertrophy in mice by calcineurin inhibition.*Science* **281**, 1690–1693.

Szymczak AL, Workman CJ, Wang Y, Vignali KM, Dilioglou S, Vanin EF & Vignali DA (2004). Correction of multi-gene deficiency in vivo using a single 'self-cleaving' 2A peptide-based retroviral vector. *Nat Biotechnol* **22**, 589–594.

Takao K, Okamoto K, Nakagawa T, Neve RL, Nagai T, Miyawaki A, Hashikawa T, Kobayashi S & Hayashi Y (2005). Visualization of synaptic Ca^{2+}/calmodulin-dependent protein kinase II activity in living neurons.*J Neurosci* **25**, 3107–3112.

Tay LH, Griesbeck O & Yue DT (2007). Live-cell transforms between Ca^{2+} transients and FRET responses for a troponin-C-based Ca^{2+} sensor. *Biophys J* **93**, 4031–4040.

Tung L & Zhang Y (2006). Optical imaging of arrhythmias in tissue culture.*J Electrocardiol* **39**, S2–S6.

van Berlo JH, Maillet M & Molkentin JD (2013). Signaling effectors underlying pathologic growth and remodeling of the heart.*J Clin Invest* **123**, 37–45.

Wilkins BJ, Dai YS, Bueno OF, Parsons SA, Xu J, Plank DM, Jones F, Kimball TR & Molkentin JD (2004). Calcineurin/NFAT coupling participates in pathological, but not physiological, cardiac hypertrophy. *Circ Res* **94**, 110–118.

Wolska BM (2009). Calcineurin and cardiac function: is more or less better for the heart? *Am JPhysiol Heart Circ Physiol* **297**, H1576–H1577.

Yang SA & Klee CB (2000). Low affinity Ca^{2+}-binding sites of calcineurin B mediate conformational changes in calcineurin A. *Biochemistry* **39**, 16147–16154.

Yang Y, Guo T, Oda T, Chakraborty A, Chen L, Uchinoumi H, Knowlton AA, Fruen BR, Cornea RL, Meissner G & Bers DM (2014). Cardiac myocyte Z-line calmodulin is mainly RyR2-bound, and reduction is arrhythmogenic and occurs in heart failure. *Circ Res* **114**, 295–306.

Additional information

Competing interests

No conflicts of interest.

Author contributions

D.T.Y. and H.B. designed the sensors and the linkers, and refined the experiments and hypothesis. H.B. performed the experiments, and carried out extensive analysis and mathematical modelling. L.J.S. contributed to the experiments and analysis in HEK cells. R.M. and I.E.D. isolated adult myocytes. I.E.D. and W.Y. contributed to adenoviral vector development. H.B., I.E.D. and L.J.S. wrote the paper utilizing D.T.Y.'s analysis and figures.

Funding

This study was supported by grants from NHLBI (D.T.Y), and the Kleberg Foundation (D.T.Y).

Acknowledgements

Over the years, we have been deeply inspired and touched by the kindness and generosity of our mentor Dr David Yue. We are grateful to have had the chance to work with him and learn from his profound and penetrating scientific vision. His death has left a deep scar in our hearts and in the field of calcium signalling. Dr Nancy Yue has been a strong advocate and supporter of the lab throughout the years and especially during this difficult time. We are inspired by her strength and are deeply grateful to her. We also thank Dr Don Bers and Dr Loren Looger for informative comments and discussions, Dr Manu Ben-Johny for optical imaging support and Dr Ting Liu and Dr Brian O'Rourke for providing resources, and assistance with aGPVM isolations. We thank all members of the Calcium Signals Lab (CSL) for their support throughout the years.